RSC Advances

ROYAL SOCIETY OF CHEMISTRY

www.rsc.org/advances

Fabrication of pH Responsive DOX Conjugated PEGylated Palladium Nanoparticle Mediated Drug Delivery System: an *in vitro* and *in vivo* Evaluation

Krishnamurthy Shanthi,[a] Karuppaiya Vimala,[a] Dhanaraj Gopi,[c] Soundarapandian Kannan[b,*]

[a] *Department of Zoology, Bharathiar University, Coimbatore-641 046, Tamil Nadu, India*

[b] Proteomics and Molecular Cell Physiology Laboratory, *Department of Zoology, Periyar University, Salem-636 011, Tamil Nadu, India*

[c] *Department of Chemistry, Periyar University, Salem-636 011, Tamil Nadu, India*

* Corresponding author at:
Proteomics and Molecular Cell Physiology Laboratory
Department of Zoology,
Periyar University,
Salem-636 011,
Tamil Nadu,
India.
Tel.: 0091 427 2345766 Etn 335; fax: 0091 2345124.
E-mail address: skperiyaruniv@gmail.com, sk_protein@buc.edu.in (S.Kannan).

†*Supporting information available*

Details on the hydrodynamic diameters and surface zeta potential value of PEGylated PdNPs and DOX conjugated PEGylated PdNPs, the cytotoxicity of PEGylated PdNPs against HeLa cells as determined by MTT assay, Cellular uptake and intracellular localization of free DOX and DOX conjugated PEGylated PdNPs in HeLa cells observed by fluorescence microscopy. The cellular and nuclear uptakes of free DOX and DOX conjugated PEGylated PdNPs in HeLa cells. Tables showing the characteristics of PEGylated PdNPs and DOX conjugated PEGylated PdNPs and percent haemolysis for positive control, negative control, PEGylated PdNPs and DOX conjugated PEGylated PdNPs at different concentrations for 3 h are given.

Abstract

Efficient delivery of therapeutics into tumor cells to increase the intracellular drug concentration is one of the key issues in cancer therapy. In this work, we designed a pH responsive PEGylated palladium nanoparticle (PdNP) as an anticancer drug nanocarrier system for effective drug delivery. The synthesis of nanocarrier involved conjugation of Doxorubicin (DOX) to the surface of PEGylated PdNPs *via* hydrazone interaction. The nanoparticles were characterized by UV-Spectroscopy, Transmission Electron Microscopy (TEM), Dynamic Light Scattering (DLS), zeta potential, Fourier Transmission Infrared Spectroscopy (FT-IR), X-Ray Diffraction (XRD) and Nuclear Magnetic Resonance (NMR). The drug release behavior was subsequently studied at different pH conditions. Result showed a sustained release of DOX preferentially at the desired endosomal pH (5.5). The biological activity of the DOX-conjugated PEGylated PdNPs was studied by MTT assay, fluorescence microscopy, and apoptosis. Intracellular-uptake studies revealed preferential uptake of these NPs into HeLa cancer cells. The *in vitro* apoptosis study revealed that the DOX-conjugated PEGylated PdNPs caused significant death to the HeLa cells. Further, blank PEGylated PdNPs displayed low toxicity and good biocompatibility. DOX-conjugated PEGylated PdNPs had the strongest anti-tumor efficacy against HeLa tumor xenograft models *in vivo*. These findings demonstrated that PEGylated PdNPs were deemed as a potential drug nanocarrier for cancer therapy.

***Keywords*:** PEGylated Palladium nanoparticles, Doxorubicin, Cytotoxicity, HeLa Cells, Apoptosis.

1. Introduction

Over the past few decades, growth of nanotechnology has developed to such an extent that it is feasible to synthesize, characterize and modify the functional properties of nanoparticles for biomedical applications.[1] This has led to an enormous interest in wide-scale production of nanoparticles (for example quantum dots, and metallic, magnetic, and polymeric nanoparticles) with different shapes and sizes for diverse biomedical applications in drug delivery, disease diagnostics, and medical imaging.[2] The limitations of conventional chemotherapy include general systemic distribution of drug, lack of drug specificity to the tumor site, insufficient local drug concentration in the tumor and poor control over drug release. The general systemic distribution of chemotherapeutic agent results in toxic side effects since the drug attacks the normal, healthy cells together with the tumor cells.[3] Therefore, it is very crucial to selectively target chemotherapeutic agents to the tumor. This need has aggravated a search for methods of drug delivery which can tackle this limitation and provide more effective cancer therapy. Delivery of chemotherapeutic agents within or conjugated to nanoparticles is a promising alternative to evade the problems associated with conventional chemotherapy.[4] In many cases, these nanoparticles often require surface modification to guarantee their biocompatibility and/or improve the bioavailability. Generally metal nanoparticles are coated with surfactants[5, 6] or polymers[7] to provide stabilization of nanoparticles in biological suspension, functionalization at the surface with drugs and to increase circulation time by reducing immediate clearance of the carriers by reticuloendothelial system (RES). Nanoparticle-based drug delivery systems have shown a high degree of efficacy in cancer treatments due to their improved pharmacokinetics and biodistribution profiles by means of the enhanced permeability and retention (EPR) effect.[8] Although the EPR is effective in enhancing the accumulation of nanoparticles (NPs) within tumor tissues, the poor cellular internalization and insufficient drug release limits the dosages of

anticancer drugs to levels below the optimum therapeutic value, thereby adversely affecting the efficacy of the chemotherapy treatment of cancer.[9] In order to address these issues, stimuli-responsive delivery systems have been explored to improve bioavailability of a drug.[10] As well, among the stimuli, pH-responsiveness is the most frequently investigated since pH values vary quite significantly in different tissues and cellular compartments.[11–13] The extracellular environment of a tumor has a lower pH (~6.8) than blood and normal tissues (pH 7.4)[14–17] whereas those of late endosome and lysosome are even lower (~5.0− 5.5).[18] Thus pH-sensitive delivery systems are of particular interest in controlled drug-delivery as evident from the literature.[19] In this context, we aimed to design a potentially capable pH- responsive nanoparticle drug delivery system specifically to cancer cells.

Among the metal nanoparticles, PdNPs belonging to the platinum group metals have been widely investigated because they exhibit unusual optical, electronic, and chemical properties, depending on their size and shape, thus opening many possibilities with respect to technological applications. The high surface to volume ratio of nanomaterials makes them highly efficient as potential catalysts. Surface plasma resonance (SPR) is another important feature in palladium nanoparticles which is useful in sensing, chemo-optical transducers, plasmonic wave guiding. [20-22] Owing to these unique properties, Pd has been used as a catalyst to manufacture pharmaceuticals,[23] degrade harmful environmental pollutants,[24] and as sensors for the detection of various analytes. [25-27] Additionally, Pd and Pd^{2+} ions also play a fundamental role in several biotechnological processes. More recently, PdNPs have been found to have antimicrobial properties.[28] Notably, PdNPs show very broad absorption through the UV-Vis-NIR region. This broad absorption nature has attracted extensive interest in using PdNPs in photothermal therapy. Xiao *et al* prepared Pd NPs with porous structure, which exhibit superior performance in

photothermal therapy compared to solid Pd nanocubes in HeLa cells.[29] In addition, a few literatures authenticated the anticancer activity of Pd complexes along with Pt (II) complex.[30,31] Furthermore, the anti-invasive property of Pd complex was also witnessed in earlier studies.[32-34] While the advantages and uses of Pd are extensive, advances are yet to be uncovered as the metals are reduced to the nanoscale. Moreover, despite the myriad applications of PdNPs in various fields, relatively no studies have been conducted to determine the therapeutic applications of PdNPs. Thus for PdNPs, there is much room for exploring their potential properties in the fields of drug delivery and it is also important to determine a baseline of toxicity for PdNPs as well as examine their potential for therapeutic applications.

Herein we introduce a novel PdNPs hybrid system to investigate their biological responses against cervical cancer. The critical part of the hybrid system is the functionalization of PdNPs surface properties by Poly (ethylene) glycol (PEG)-hydrazide polymers and conjugating DOX onto the PEG-hydrazide (PEGylated) PdNPs. Hydrophilic polymer PEG was chosen as surface modifiers of PdNPs because of its biocompatibility.[35] PEG coated nanoparticle surfaces when dispersed reduce nonspecific protein adsorption and clearance by macrophages, and render the nanoparticles capable of crossing the cell membrane. [36, 37] DOX was chosen as a model anti-cancer agent owing to its high therapeutic index and better activity against a wide spectrum of tumors.[38] In the present study, our goal is to conjugate DOX with PEGylated PdNPs nanocarriers and study the drug loading and controlled release profile from these nanocarriers. Additionally, the targeting activity of the nanoparticles in HeLa cancer cells was evaluated by cellular uptake and cytotoxicity *in vitro*. The targeting characteristics of DOX conjugated PEGylated PdNPs were further investigated by anti-tumor efficacy studies *in vivo*. The process involved in the fabrication of PEGylated PdNPs, can be used to conjugate with DOX *via*

hydrazone bond. When the as-fabricated nanoparticles targeted the HeLa cells, the nanoparticles enter into the cytoplasm mediated by endocytosis effects. DOX is then released from nanoparticles at low pH which degrades polymer and resulting in inhibition of tumor cell growth through apoptosis.

2. Experimental

2.1. Materials

The human cervical cancer cell line (HeLa) was procured from National Center for Cell Science (NCCS, Pune), Palladium (II) chloride ($PdCl_2$) as the source of palladium ions, methoxy poly(ethylene glycol)–succinimidyl (5k) (PEG–SCM), triethylamine (TEA), 3-(4,5-dimethylthiazolyl-2)-2,5-diphenyltetrazolium bromide (MTT), 4′-6-diamidino-2-phenylindole (DAPI), acridine orange/ethidium bromide (Ao/EtBr), tetrahydrofuran (THF), sodium borohydrate ($NaBH_4$), Sodium dodecyl sulphate (SDS) and hydrazine was purchased from Sigma–Aldrich (Bangalore). Analytical grade reagents were purchased from Sigma–Aldrich (Bangalore). All the samples were prepared in Milli-Q water.

2.2. Synthesis of DOX conjugated PEGylated PdNPs *via* Hydrazone Bonds

2.2.1. Synthesis of PEG–hydrazine

The typical synthesis of PEG–hydrazine was as follows: 600 mg of methoxy PEG (5k) succinimidyl carboxymethyl ester and 160 mg of hydrazine were dissolved in 10 mL phosphate buffer solution (PBS) (pH 7.4) and stirred for 24 h. The product was then dialyzed against distilled water for 2 days to remove the excess hydrazine molecules. The final product was obtained by lyophilization and the yield was 90%.

2.2.2. Preparation of PEGylated PdNPs

Typically, 0.1780 g of $PdCl_2$, 12 mL of 0.2M HCl and 500 mL of distilled water were mixed to get H_2PdCl_4 (Dihydrogentetrachloropalladate II) solution with a concentration of

2 mM. Then, the total volume was put in a flask, refluxed for 3 h and allowed to age for 2 days. The color of the product was typically pale-yellow. Then, to 30 mL of 2mM H_2PdCl_4 , 0.1334 g of PEG–hydrazine was added and stirred at room temperature (27 ± 1^0C) for 10 min. An aqueous solution of $NaBH_4$ (0.01 M) was added drop by drop to this mixture and the formation of the PEGylated PdNPs was observed as an instantaneous colour change of the solution from pale yellow to dark brown after the addition of a reducing agent along with surfactant (1mM SDS). The as-prepared PEGylated PdNPs were separated by centrifugation at 15,000 rpm for 10 min, washed several times with water, and then dried at 60 ºC for 5 h in a vacuum dryer or re-dispersed in water to produce a colloidal suspension for further characterizations.

2.2.3. Preparation of DOX conjugated PEGylated PdNPs and Drug Loading Content

Before conjugating DOX onto the PEGylated PdNPs, 5 mg of DOX.HCl was stirred overnight with twice the number of moles of TEA in 10 mL of DMSO to obtain the DOX base. To the obtained DOX base, PEGylated PdNPs (50 mg) was added, which was stirred at room temperature for another 2 h to allow the formation of the hydrazone linkage between C-13 carbonyl group of DOX and the hydrazide moiety on the nanoparticles. The final mixture was transferred to a dialysis tube (MWCO 5000 Da) and dialyzed against ultrapure water at 25 ºC for 24 h. During the first 12 h, the water was exchanged three times (every 4 h) and then twice during the following 12 h. Afterwards, the solution in the dialysis tube was filtered through a syringe filter (pore size = 0.45 μm) to remove the unloaded DOX, and then collected by freeze-drying. The entire procedure was performed in the dark. The DOX concentration in DMSO was determined by fluorescence measurement using a calibration curve constructed from DOX/DMSO solutions with different DOX concentrations. The drug loading content (DLC) was calculated according to the following formula:

DLC (wt %) = (weight of loaded drug/weight of drug - loaded carrier) x100%

2.3. Characterization of Nanoparticles

2.3.1. UV-visible Spectroscopic Studies

The change in surface plasmon resonance of PEGylated PdNPs, before and after loading of DOX, was monitored by UV-Visible spectroscopy measurements, carried out on a Shimadzu UV–*vis* Spectrophotometer. The optical properties were monitored in 10 mm optical path-length-quartz-cuvettes over wavelengths from 200 to 800 nm. Equivalent amounts of the suspension (0.5 mL) were diluted in a constant volume of deionized water (5 mL) and subsequently analyzed at room temperature.

2.3.2. Transmission electron microscopy

Morphological examination of the nanoparticles was examined by Transmission Electron Microscopy (TEM) (Hitachi 7000H, Tokyo, Japan) operated at an accelerating voltage of 120 kV. Samples for TEM studies were prepared by placing a drop of colloidal dispersion on the carbon-coated copper grid, followed by evaporating off the solvent under vacuum conditions.

2.3.3. Particle size analysis and zeta potential measurement

Dynamic light scattering and zeta potential experiments were conducted on 6.32 Ver. Zetasizer particle size analyzer (MAL1037088 Malvern Instruments Ltd). The machine was calibrated using a 60 nm polystyrene standard. Prior to the loading of the sample, the colloidal solution was sonicated for 1 min to produce better particle dispersion and to prevent nanoparticle agglomeration. The hydrodynamic diameter and the surface charge of PEGylated PdNPs before and after loading of DOX were measured in triplicate. Calculation of the size and polydispersity indices was achieved using the software provided by the manufacturer.

2.3.4. X-Ray diffraction studies

NPs were set onto the slides of special glass for the X-ray diffraction (XRD) method with an area ~1 cm^2. The drops of NPs were placed on glass and air dried prior to use. These slides were treated with ethanol to remove any impurities. XRD patterns were recorded by a diffractometer (X'Pert – Phillips) operating at 45 kV/45mA and using Cu-Kα radiation (1.54056 Å). The scan was taken between 2θ of 10° and 2θ of 45° at increments of 0.04° with a count time of 4 sec for each step. The lattice parameters are calculated from the formula:

$$\frac{1}{d^2} = \frac{h^2 + k^2 + 1^2}{a^3}$$

The average grain size of the PEGylated PdNPs and the DOX conjugated PEGylated PdNPs is calculated using Scherrer formula:

$$D = \frac{0.89\lambda}{\beta\ Cos\theta}$$

Where D is the crystallite size, λ is the wavelength (1.5406 Å for Cu Kα), β is the full-width at half-maximum (FWHM) of main intensity peak after subtraction of the equipment broadening and θ is the diffraction angle.

2.3.5. Fourier Transform Infrared Spectroscopy

FTIR spectra of PEGylated PdNPs, free DOX and DOX conjugated PEGylated PdNPs were analyzed by FTIR spectroscopy (Shimadzu 8400S, Japan) using a KBr compressed pellet method in the transmission mode at 4 cm^{-1} resolution. The various modes of vibrations were identified and assigned to determine the different functional groups on the nanoparticle.

2.3.6. Nuclear Magnetic Resonance

The chemical structure of the as-synthesized NPs was next characterized by ^{1}H NMR analysis. ^{1}H-NMR spectra were recorded using a Perkin Elmer Instrument- 400MHz with DMSO as the solvent.

2.4. *In-vitro* drug release response

The drug release response from polymer modified nanoparticles was investigated at the physiological temperature of 37 °C and pH of 7.4, 6.8 and 5.5. The medium of pH 7.4 corresponds the physiological pH while pH 6.8 simulates the pH of tumor tissue and pH of 5.5 corresponds to the mature endosomes of tumor cells. The release profiles of DOX from PEGylated PdNPs were studied using a dialysis bag (MWCO-3500). Briefly DOX conjugated PEGylated PdNPs was dispersed in 10 mL of the respective PBS buffer, allowed to stabilize for 30 min, and then placed in a dialysis bag. The dialysis bag was immersed in 50 mL of PBS solution (pH 7.4, 6.8, or 5.5) in a beaker and then placed in a 37 °C water bath shaker at 110 rpm. At predetermined time intervals, 3mL of the release medium was collected to measure the released drug concentration and then was replaced with the same fresh PBS. For the measurement of released DOX concentration, the absorbance of the release medium at 480 nm was recorded on a Shimadzu UV–*vis* absorption spectrophotometer. Experiments for all samples were performed three times at each pH value.

2.5. *In vitro* cytotoxicity study

Cytotoxicity of DOX-free PEGylated PdNPs and DOX-conjugated PEGylated PdNPs against HeLa cells was assessed *in vitro* by MTT assay. This assay is based on the ability of live cells to convert the MTT (solution of yellow color) into blue formazan salts. Briefly, HeLa cells were seeded into a 96-well plate at a density of 5.0×10^{3} cells/well in 100 µL of complete DMEM containing 10% FBS. The cells were cultured for 1 day at 37 ºC in 5% CO_2 atmosphere.

Afterwards, the cells were incubated with PEGylated PdNPs, DOX-conjugated PEGylated PdNPs, or free DOX for 48 h at 37 ºC. The concentrations of DOX-free PEGylated PdNPs ranged from 3.125μg/mL to 200 μg/mL. DOX-conjugated PEGylated PdNPs or free DOX were diluted in complete DMEM with final DOX concentrations from 0.125 μg/mL to 8 μg/mL. After incubation, MTT stock solution (5 mg/mL in PBS, 20 μL) was added to each well and incubated for 4 h. The media were completely removed and 150 μL of DMSO was added to each well to dissolve the formazan blue crystal and the absorbance was monitored using a microplate reader (Bio-TekELx800) at the wavelength of 490 nm. The cytotoxicity was expressed as the percentage of cell viability compared to untreated control cells. All experiments were repeated three times.

2.6. Cellular Uptake of DOX conjugated PEGylated PdNPs

CLSM was used to examine the intracellular distribution of DOX. HeLa cells were seeded on slides on a 24-well plate at a density of 5.0 x 10^4 cells/well in 1 mL of complete DMEM containing 10% FBS. The cells were cultured for 1 day at 37 ºC in 5% CO2 atmosphere. The cells were then incubated with DOX-conjugated PEGylated PdNPs at a final DOX concentration of 2 μg/mL in DMEM for 2 or 24 h at 37 ºC. At each predetermined time, the culture media were subsequently removed and the cells were washed with PBS (1 min x 3) to remove DOX-loaded micelles that were not ingested by the cells. Thereafter, the cells were fixed with 4% (w/v) paraformaldehyde aqueous solution for 10 min at room temperature. The slides were then rinsed with PBS (5 min x 3). Finally, the cells were stained with DAPI (5 mg/mL in PBS) at 37 ºC for 8 min, and the slides were rinsed with PBS (5 min x 3). The prepared slides were examined by CLSM (Nikon, TE2000, EZ-C1, Japan).

For fluorescence microscopic study, HeLa cells were seeded in a 24-well plate and incubated for 24 hours to allow the cells to attach. A certain amount of free DOX and DOX

conjugated NPs (DOX concentration 2 μg/mL) were added, and the cells were further incubated for 48 hours. After washing the cells with PBS (pH 7.4) three times, the cellular uptake was observed by fluorescence microscope (DMIL; Leica Microsystems Ltd, Wetzlar, Germany).

2.6.1. Flow cytometry measurement.

To obtain a quantitative cellular uptake of DOX for DOXconjugated PEGylated PdNPs, HeLa cells were cultured with DOX or DOXconjugated PEGylated PdNPs in a 24- well plate at the density of 5.0 x 10^4 cells/well for 48h. The cells were then washed with PBS three times and harvested. The cells were re-suspended in PBS buffer (10 mM) and fixed with cold 70% ethanol aqueous solution overnight for flow cytometric measurement.

2.6.2. Cellular and nuclear quantification of doxorubicin

HeLa cells were exposed to free DOX and DOX conjugated PEGylated PdNPs (DOX concentration 2μg/mL) for 2, 12, 24 and 48h. HeLa cells, released by typsinization, were suspended at a concentration of 5.0 x 10^6 cells/ml for 10 min at 4 °C in a 100 mM NaCl solution with 1 mM EDTA, 1% Triton X-100 (Sigma Chemical Co.), and 10 mM Tris buffer (pH 7.4) The suspension was then centrifuged and the resulting precipitate of cell nuclei was separated from the supernatant cell cytosol. DOX was extracted from both fractions by treatment with 0.075N HCl in 90% isopropyl alcohol at 4 °C overnight. The mass of DOX in the HeLa cells nuclei was measured by UV-*vis* at absorption wave number of 480 nm.

2.7. AO/EtBr staining assay

Approximately 1 μL of a dye mixture (100 mg/mL acridine orange (AO) and 100 mg/mL ethidium bromide (EtBr) in distilled water) was mixed with 9 mL of cell suspension (1×10^5 cells/mL) on clean microscope cover slips. The cancer cells were collected, washed with phosphate buffered saline (PBS) (pH 7.2) and stained with 1 mL of AO/EtBr. After incubation

for 2 min, the cells were washed twice with PBS (5 min each) and visualized under a fluorescence microscope (Nikon Eclipse, Inc, Japan) at 400× magnification with an excitation filter at 480 nm.

2.8. DAPI Staining for Nuclear Morphology Study.

For visualization of HeLa cells, the nuclei of the cells were stained with DAPI. The efficiency of DOX conjugated PEGylated PdNP was tested through apoptosis study. For this purpose, HeLa cells were treated with nanoparticles at their different concentration for 24 h at 37 °C. Then, cells were fixed with 4% paraformaldehyde for 15 min, permeabilized with 0.1% Triton X-100, and stained with 1 mg/mL DAPI for 10 min. The cells were then rinsed with PBS and morphological changes were analyzed under fluorescence microscopy (Nikon Eclipse, Inc., Japan) at 400× magnification with excitation filter at 510–590 nm. The percentage of total apoptotic cells was determined by the following formula:

$$\%\ \text{of apoptotic cells} = \frac{\text{Total number of apoptotic cells}}{\text{Total number of normal and apoptotic cells}} \text{X } 100$$

2.9. Semi-quantitative RT-PCR analysis

RT-PCR analysis was used to examine the expression levels of Bcl-2, cytochrome C and caspase 3 and 9 mRNA. RT-PCR for β-actin was also independently performed as an internal control. The total RNA was isolated using the TRIzol reagent (Sigma–Aldrich) according to the manufacturer's instructions and reverse transcribed. Briefly, the cDNA was amplified in a 50 µL reaction containing primer pairs (1.0 µL):10× buffer (5.0 µL), cDNA (2.0 µg), and 25 mmol/L MgCl (3.0 µL), 10 mmol/L dNTPs (1.0 µL), and Taq polymerase (2.5 U). Semi-quantitative RT-PCR amplification cycles consisted of denaturation at 94 °C for 1 min, primer annealing at 57 °C for 45 s and extension at 72 °C for 45 s, for a total of 30 cycles followed by final extension

at 72 °C for 10 min. The PCR product was separated on 1.5% agarose gels. The primer sequences used for PCR were:

Gene product	Primers sequences	Product Size (bp)
Bcl2	sense 5′- CCAAGCTGAGCGAGTGTC- 3′and anti-sense 5′-ACAAAGATGGTCACGGTCTGCC-3′	415
Caspase 3	sense5′-GACAACAACGAAACCTCCGT-3′and anti-sense 5′- GACTTCGTATTTCAGGGCCA-3′	382
Caspase 9	sense 5′- TGTGGTGGTCATCCTCTCTCA-3′and anti-sense 5′-GTCACTGGGGGTAGGCAAACT-3′	282
Cyto C	sense 5′-GGAGGCAAGCATAAGACTGG-3′ and anti-sense 5′-GTCTGCCCTTTCTCCCTTCT-3′	170
β-actin	sense 5′ AACCGCGAGAAGATGACCCAGATCATGTTT-3′ and anti-sense 5′-AGCAGCC GTGGCCATCTCTTGCTCGAAGTC-3′	350

2.10. Hemolytic assay

Ethylenediamine tetraacetic acid (EDTA)-stabilized human blood samples were freshly collected and used within 3 h of being drawn. A 4 mL sample of whole blood was added to 8mL of phosphate-buffered saline (PBS). The PBS solution was formulated to the following composition (mM): 0.14 NaCl, 2.7 KCl, 10 Na_2HPO_4, and 1.8 KH_2PO_4. NaOH was added to the PBS solution to adjust the pH to 7.4 as measured by a calibrated, pH meter (320, Corning Inc., Corning, NY). The RBCs were isolated from serum by centrifugation at 10016g for 5 min. The RBCs were further washed five times with sterile PBS solution. Following the last wash, the RBCs were diluted to 40 mL of PBS. Then 0.2 mL of diluted RBC suspension was added to PEGylated PdNP and DOX conjugated PdNP solutions at systematically varied concentrations and mixed by vortexing. All the sample tubes were kept in static condition at room temperature for 3 h. Finally, the mixtures were centrifuged at 10016*g* for 3 min, and 100 μL of supernatant of all samples was taken, and its absorbance was recorded on a spectrophotometer (Shimadzu UV–*vis* Spectrophotometer) at 545 nm. The percentage hemolysis was calculated using the following relationship.

$$\text{Hemolysis \%} = \frac{\text{Sample absorbance} - \text{negative control}}{\text{Positive control} - \text{negative control}} \text{ X } 100$$

Herein, RBC incubation with D.I. water and PBS were used as the positive and negative controls, respectively.

2.11. Assessment of Anti-tumor Activity *in vivo*.

The anti-tumor efficiency of DOX conjugated PEGylated PdNPs was assessed in tumor-induced mice. Briefly, the subcutaneous dorsa of BALB/c female nude mice were inoculated with HeLa cells (1×10^7) in 100 µL of normal saline. When the volume of the xeno-graft tumor reached approximately 70-100mm^3 the mice were randomly divided into four groups with six mice in each group: group A, normal saline; group B, free DOX; group C, PEGylated PdNPs; group D, DOX conjugated PEGylated PdNPs. Various DOX formulations with the drug concentration of 5 mg/kg was injected intravenously every 2 days, and the mice were then observed for 18 days. The tumor diameters were measured every 3 days interval for each group. The tumor volumes (V) and body weight were calculated using the formula $V = [\text{length} \times (\text{width})^2]/2$. For the assessment of toxicity, organs such as, liver, heart, kidney, lung, and spinal cord were collected, fixed in 4% paraformaldehyde solution and made into 4 mm sections which were stained with hematoxylin and eosin (H&E) and observed under a microscope. All experiments were performed in compliance with the relevant laws and institutional guidelines (Animal Ethical Committee, Periyar University, Salem) and this work has been approved by the IAEC (Institutional Animal Ethical Committee) constituted as per the Rules and Regulations of Ministry of Animal Husbandry, Government of India.

3. Statistical analysis

All the measurements were made in triplicate and all values were expressed as the mean ± standard error. The results were subjected to an analysis by Student's t-test. The results were considered statistically significant if the *p*-value was ≤ 0.05.

4. Results and discussion

4.1. Synthesis and characterization of DOX-conjugated PEGylated PdNPs

Hydrazone bond was employed in this work to connect DOX, as it is more sensitive to tumor microenvironments than other covalent linkers. The negatively charged group of oxygen in PEG-hydrazide could react with H_2PdCl_4, which were reduced to become Pd atoms by adding $NaBH_4$ (reducing agent). The accumulating Pd atoms leads to the formation of PdNP, thus PEG assembled to be absorbed to the surface PdNPs, leaving the hydrazine group outward. Meanwhile DOX was conjugated onto the as-synthesized PEGylated PdNPs through hydrazine linkage formed between the carbonyl groups of DOX and hydrazine side groups of PEGylated PdNPs. The reaction scheme for the synthesis of DOX-conjugated PEGylated PdNPs is shown in scheme 2.

4.1.1. Visual observations.

Reduction of the aqueous Pd ions was tracked by monitoring changes in color. The reaction media offered a change in color from pale yellow (Pd^{2+} ion solution) to dark brown after complete reduction of H_2PdCl_4 (insert of Fig.1a) indicating the generation of PdNPs. The same accreditation was made by Teranishi and Miyake [39] during the formation process of PVP-protected Pd nanoparticles and Xin yang *et al* [40] during the rapid reduction of $PdCl_2$ using *Cinnamomum camphora* leaf. The intensity of the color arises from the surface plasmons, which

are dipole oscillation arising when an electromagnetic field in the visible range is coupled to the collective oscillations of conduction electrons. [41]

4.1.2. UV–*vis* spectroscopy studies

The UV-*vis* spectra of H_2PdCl_4, and PEGylated PdNPs are displayed in Fig. 1a. As can be seen, the UV-*vis* spectra of H_2PdCl_4 reveal a peak around 425 nm which refers to the existence of Pd^{2+} ions.[40] The reduction process as monitored using UV visible spectra for PEGylated PdNPs shows that the peak at 425 nm was entirely removed indicating complete reduction of Pd^{2+} ions to PdNPs . The absence of the absorption peaks above 300 nm shows the full reduction of the initial Pd(II) ions. [42,43] Yonezawa *et al.* [44] have ascribed the absence of absorption bands to the total reduction of Pd(II). The same assignment was made by Ho *et al*.[45] during thermally reduced-induced reduction of Pd (fod) 2. The spectra of the PEGylated PdNPs present broad continuous absorptions in the UV-visible range. These absorptions are typical of those of colloidal palladium.[42, 46]

The UV-*vis* spectra for bare DOX and DOX conjugated PEGylated PdNPs is presented in Fig. 1b. The bare DOX shows peaks at 232, 262, 290 and 490 nm.[47] The conjugation of DOX onto the PEGylated PdNPs was evident from the spectrum of DOX conjugated PEGylated PdNPs solution, which clearly shows the characteristic absorption peaks of DOX. Moreover, these peaks showed red-shifts. For example, the peaks of DOX at 232, 262 and 490 nm shifted to 234, 265 and 501 nm after interaction with PEGylated PdNPs.

4.1.3. X-ray diffraction pattern

The crystal structure and phase purity of PEGylated PdNPs and DOX conjugated PEGylated PdNPs were studied using X-ray diffraction pattern (Fig. 2). The diffraction peaks at 40.11^o and 46.01^o can be index to (111) and (200) planes of face centered cubic (fcc) structure of PdNPs and well matched with the Standard JCPDS data (89 - 4897). The peaks observed at

20.05 ^{0} and 25.38 ^{0} (Fig. 2a) are due to the presence of PEG moieties.[48] All other diffraction peaks observed in Fig. 2b might be due to the presence of DOX. The estimated average lattice constants are a=3.889 Å which is consistent with the standard JCPDS data. The calculated grain size of PEGylated PdNPs and DOX conjugated PEGylated PdNPs are 17.8 and 40.7nm respectively. Compared to PEGylated PdNPs the grain size of DOX conjugated PEGylated PdNPs is increased which is due to the conjugation of DOX onto the PEGylated PdNPs.

4.1.4. TEM, DLS and Zeta Potential

The morphology and size of the nanoparticles were characterized using TEM and DLS. The micrographs of PEGylated PdNPs and DOX conjugated PEGylated PdNPs are shown in Fig. 3. Most of the PEGylated PdNPs and DOX conjugated PEGylated PdNPs were fairly spherical in shape. The observed size of PEGylated PdNPs ranged approximately between 10- 20 nm and those of DOX conjugated PEGylated PdNPs presented a slightly large size of approximately 35-45 nm. The hydrodynamic diameters of prepared nanoparticles measured by DLS were 17 ± 2 nm (PDI = 0.127±0.09) for PEGylated PdNPs and DOX conjugated PEGylated PdNPs were 40 ± 5 nm (PDI = 0.214±0.01) as shown in Fig. S1. The smaller hydrodynamic diameter and the narrow size distribution of PEGylated PdNPs (without DOX) indicated the formation of hydrazone bond during the particle formation step of DOX-conjugated PEGylated PdNPs, possibly due to the presence of DOX molecules, leading to the formation of bigger particles with larger polydispersity. Hence upon addition of DOX, the PEGylated PdNPs increased in size which may be due to the conjugation of DOX to the NPs surface. Furthermore, drug carriers of diameters larger than 200nm are readily scavenged nonspecifically by monocytes and the reticuloendothelial system.[49] It was reported that smaller particles tended to accumulate at the tumor sites because of the EPR effect [50] with greater internalization.[51] DOX conjugated PEGylated PdNP are thus convenient to benefit from the EPR effect and ideal for targeting

tumors. Stability of the nanoparticles is vital for biomedical applications. Surface zeta potential is closely related to the stability of NPs. The zeta potential of nanoparticles were negative and ranged about −32.8 ± 0.27 mV for PEGylated PdNPs and -36.7 ± 0.65 mV for DOX conjugated PEGylated PdNP (Fig. S2). The excess negative charge of PEGylated PdNPs orients from unbound surfactant molecules (0.1% SDS) thereby leading to more negative zeta potential values. Mandal *et al.* [52] obtained silver nanoparticle with zeta potential of −21.7mv using functionalized PEG while adding triton X-100 as surfactant. The excess negative charge was due to triton X-100 surfactant. Illes *et al*.[53] obtained negative charged nanoparticals upto -40mV on increasing the amount of PEG polymer. Brarara *et al*.[54] also obtained nanoparticle with zeta potential of -35mv using functionalized PEG. It was reported that NPs with negatively charged surface showed a reduced plasma protein adsorption and low rate of nonspecific cellular uptake.[55,56] Meanwhile, the charged NPs can repel one another to overcome the natural tendency of aggregation of NPs.[57] Thus, PEGylated PdNPs and DOX conjugated PEGylated PdNP had enough dispersion stability in aqueous solution and favorable for accumulation in the tumor tissue by EPR effect.

4.1.5. FTIR and NMR analysis

FTIR is an appropriate technique to ascertain the attachment of the polymer to the PdNPs and conjugation of drug with the PEGylated PdNPs. Fig. 4 shows the FTIR spectra of PEGylated PdNPs , DOX and DOX conjugated PEGylated PdNPs . In case of PEGylated PdNPs, the band at 3432 cm^{-1} is assigned to O-H stretching (ν) vibrations. The bands at 2922 cm^{-1} corresponding to C–H stretching vibrations, at 1730 cm^{-1} corresponding to C=O stretching vibrations, at 1401 cm^{-1} attributable to $-NH_3^+$ and at 1104 cm^{-1} corresponding to C-O-C are observed in PEGylated PdNPs, confirming the attachment of PEG-hydrazide onto PdNPs. FTIR was further extended to study the conjugation of DOX with the PEGylated PdNPs. FTIR spectrum of pure

DOX shows peaks at 3450 cm^{-1} due to N–H stretching vibrations for the primary amine structure and at 3330 cm^{-1} due to O–H stretching vibrations. However, in case of DOX-conjugated PEGylated PdNPs, peak due to N–H stretching vibrations and O–H stretching vibrations overlap, are broadened and shifted to the lower frequency range (~3265 cm^{-1}).[1,58] Further when compared to the IR spectrum of DOX, the peaks at 1734 cm^{-1} corresponding to C=O disappears and C=N bond showed up at 1636 cm^{-1} indicative of hydrazone bond. The characteristic absorbance bands of 681 cm^{-1} relates to DOX. From this FTIR result, it can be interpreted that the attachment of DOX to PEGylated PdNPs occurs via the formation of hydrazone bond between the hydrazide groups of PEGylated PdNPs and the carbonyl groups of DOX.

The NMR spectra depicted in Fig. 5a authenticate the presence of PEGylated PdNPs. The respective chemical shifts peaks had been noticed at 1.98, 2.40, 3.31-3.95 minutes. Interestingly the DOX conjugated PEGylated PdNPs accentuated the characteristic peaks at 3.80, 3.47, 2.49, 1.20 minutes respectively. This signal frequency in the form of chemical shift as detected by NMR spectroscopy is proportional to the magnetic field applied to the nucleus of the DOX conjugated PEGylated PdNPs (Fig.5b). In addition the occurance of PEGylated PdNPs had been confirmed by showing the chemical shift peaks at 7.89, 7.61, 1.11, 1.02 minutes. Thus the Fig. 5b reveals the firm conjugation of DOX onto PEGylated PdNPs.

4.2. Doxorubicin (DOX) drug loading profile

To assess the feasibility of using PEGylated PdNPs as an anticancer drug carrier, we performed loading and in vitro DOX release studies using PEGylated PdNPs. DOX loading was attributed to the conjugation of carbonyl group in DOX to the surface active hydrazide group in PEGylated PdNPs. Before loading DOX onto the NPs, DOX.HCl was stirred with twice the number of moles of TEA in DMSO to detach HCl and render the drug hydrophobic. The

characteristics of DOX conjugated PEGylated PdNPs, including DLC, particle size, PDI and zeta potential are summarized in Table S1. The theoretical DLC was set at 10wt%, and the results showed that the DLC of DOX conjugated PEGylated PdNPs were 8.79wt%, implying that DOX was effectively conjugated onto the NPs. After DOX loading, PEGylated PdNPs had a larger size (approximately 40 nm) than DOX-free PEGylated PdNPs (approximately 17 nm).

4.3. *In vitro* drug release profile

Macromolecules and particles are uptaken by cells *via* endocytosis mechanism. Endocytic pathway involves acidic membrane-vesicles (endosomes and lysosomes). Besides, some tumor sites have slightly acidic extracellular environment.[59] In view of that, we aimed to synthesize a pH sensitive PEGylated DDS for the antitumor drug, DOX. The drug release response of PEGylated PdNPs was evaluated under different pH conditions, pH 7.4 (corresponds to the environment of blood), pH 6.8 (the pH of tumor tissue), and pH 5.5 (simulates the pH in mature endosomes of tumor cells) at a temperature of 37 °C. The temperature of 37 °C was selected for drug release response because it is close to the physiological temperature. As shown in Fig. 6 PEGylated PdNPs exhibited obvious pH-related release behavior. The result shows that at pH 7.4 the drug release was slow and sustained with release ratio at about 19 ± 0.23% in 48 h. The hydrazone linkage enables DOX conjugated PEGylated PdNPs to remain stable for a considerable period of time during circulation in the blood at pH 7.4 and thereby eliminates the premature burst release. Such stability, to a large extent, can reduce the side effects of the drug on normal cells. At pH 6.8, the drug release ratio was higher than that at pH 7.4; about 68 ± 0.27 % loaded drug was released due to the slight protonation. However at pH 5.5 DOX was released more rapidly with approximately 89 ± 0.34% within the same period indicating the sensitivity of DOX conjugated PEGylated PdNP to endosomal pH. At lower pH 5.5 the degradation of

493 hydrazone bonds of DOX conjugated PEGylated PdNPs contributes to the facile release of the
494 conjugated drug.
495
496 **4.4. *In vitro* cytotoxicity**
497 To evaluate the cytotoxicity of DOX conjugated PEGylated PdNP, *in vitro* cytotoxicity
498 tests of free DOX, and DOX conjugated PEGylated PdNP against human against HeLa cell line
499 were conducted for 24 h and 48 h by MTT assay at different DOX concentrations. It is well
500 known that the biocompatibility of nanoparticles is most important for biomedical applications.
501 To ensure that the toxicity of PEGylated PdNPs (DOX-free), *in vitro* cytotoxicity test for
502 PEGylated PdNPs against HeLa cells was also conducted. No appreciable deduction in cell
503 viability was observed for both 24 h and 48 h incubation, indicating that PEGylated PdNPs is
504 highly biocompatible (Fig S3). As can be seen from Fig.7, free DOX and DOX conjugated
505 PEGylated PdNPs showed dose-dependent toxicity for both 24 h and 48 h. As expected, DOX
506 delivery mediated by PEGylated PdNPs could cause substantially enhanced cytotoxicity to HeLa
507 cells. The results (Fig. 7) indicate a significant cytotoxic effect after 24 h of incubation when free
508 DOX at 2 µg/mL is used. In particular, after 24 h of incubation with free drug, the HeLa cells
509 were 50% viable, in agreement with previous literature results [60] and on further incubation for
510 48h, 50% viability was seen at even lower concentration of 1 µg/mL. Accordingly the half-
511 maximal inhibitory concentration (IC_{50}) value of free DOX was 2±0.1 µg/mL and 1.0± 0.2
512 µg/mL for 24 h and 48 h respectively. In the case of DOX conjugated PEGylated PdNP the
513 cytotoxic response was significantly higher when compared to free DOX. The IC_{50} values of
514 DOX conjugated PEGylated PdNPs were 1.0±0.3 µg/mL and 0.5± 0.1 µg/mL for 24 h and 48 h
515 respectively. These results demonstrated that DOX conjugated PEGylated PdNPs showed
516 increased toxicity compared to free DOX (*p<0.05) and exhibited significant *in vitro* antitumor

activity. This result is considered to be due to the enhanced loading of drug onto the PEGylated PdNPs and efficient internalization mediated by endocytosis. Thus DOX conjugated PEGylated PdNPs effectively decreased the *in vitro* cancer cell viability, which could imply the potential targeting effects of these nanocarriers.

4.5. Cellular uptake of DOX conjugated PEGylated PdNPs .

To verify intracellular drug release, DOX conjugated PEGylated PdNPs were monitored using confocal microscopy after treatment with HeLa cells for 24 and 48 h. As shown in Fig. 8, the distribution of DOX in cells was different at 24 and 48 h. Indeed, in 24 h, the red fluorescence of DOX conjugated PEGylated PdNPs was observed to accumulate around the nucleus inside the cells (though there was some red fluorescence diffused through nucleus) indicating that the DOX conjugated PEGylated PdNPs were initially located within the endosomal intracellular compartments, releasing cleaved DOX in the cytosol region in a sustained manner. With further incubation for 48 h, maximum DOX fluorescence could be detected in the nucleus. Full drug cleavage from the PEGylated PdNPs prodrug had taken place and almost all the drug molecules had migrated into the nucleus, over a prolonged incubation period (48 h) and they were eventually located in the nucleus. This suggested that the DOX conjugated PEGylated PdNPs entered into the cells *via* endocytosis. The same accreditation was made by Nguyen-Van Cuong [61] in MCF-7 cells incubated with DOX-loaded micelle.

The cellular uptake was further observed by fluorescence microscope after the cells were incubated with free DOX and DOXconjugated PEGylated PdNPs for 48 h. The negative control was HeLa cells without any treatment. Fig. S4a shows the fluorescence images of DOX against Hela cells with incubation times of 48 h. It was clear that at the same incubation time, the DOX fluorescence intensity in Hela cells was enhanced when DOX was conjugated to the PEGylated PdNPs. On the basis of these fluorescence images, it can be concluded that DOX conjugated to

the PEGylated PdNPs can enter into the cells and distribute throughout the nucleus more efficiently than free DOX by 48 h. An earlier report indicated that DOX fluorescence is observed only when DOX is released because of the self-quenching effect of DOX in NPs.[62] In the current work, the image indicated the release of DOX from PEGylated PdNPs and its localization in nuclei. The observation can be attributed to the cleavage of hydrazone bonds in response to the intracellular pH level of endosome. Consequently, the DOX burst release from the disruptive NPs and can be readily diffused into the nuclei. This result was consistent with the cytotoxicity of pH-sensitive DOX conjugated PEGylated PdNPs showed higher cytotoxicity because of the accumulation of DOX in its intracellular active site (nuclei), which enhanced its effect. Fig. S4b displays the mean DOX fluorescence intensity of the HeLa cells on the basis of the flow cytometry analysis. Compared with the cells incubated with free DOX, the DOX conjugated PEGylated PdNPs displays stronger fluorescence intensity. It can be seen that the fluorescence intensity of HeLA cells cultured with DOX conjugated to the PEGylated PdNPs was about 2.5 times of cells cultured with free DOX. The results clearly demonstrated that DOX conjugated to the PEGylated PdNPs enhanced the intracellular release of DOX compared with free DOX. The fluorescence signals are associated with the DOX release quantity from PEGylated PdNPs. Therefore, the enhanced intracellular DOX fluorescence in cells treated with DOX conjugated PEGylated PdNPs was due to the rapid and complete intracellular DOX release. This result was in accordance with our expectation that hydrazone bonds would be cleaved in the intracellular environment. Hence, PEGylated PdNPs was a suitable anticancer drug carrier.

To investigate quantitatively the delivery of DOX conjugated PEGylated PdNPs to the nucleus, cell fractionation experiments were done. Cellular and nuclear uptake kinetics of free DOX and DOX conjugated to the PEGylated PdNPs was examined for Hela cells at elapsed time

points, shown in Fig. S5. Cellular and nuclear uptakes of DOX conjugated to the PEGylated PdNPs were time dependent. In the case of free DOX most of the drug was found in the nuclear fraction already after 2 h of incubation. The intense DOX accumulation in the nucleus for free DOX occurred because intracellular DOX molecules in the cytosol could transport rapidly to the nucleus and intensely bound to the chromosomal DNA.[63] In fact, the drug concentration in cells treated with free DOX did not increase at all when incubation was prolonged from 2 h to 48 h. This might be due to the fact that free DOX without drug carrier releases rapidly and the release is almost completed within 8 h.[64] In contrast to free DOX, DOX conjugated PEGylated PdNPs were mainly distributed in the cytoplasm without exhibiting much accumulation in the nuclear fraction. With further incubation for 12 h, the DOX molecules inside the cells increased and the accumulation of DOX in the cytoplasmic fraction were later observed to slowly migrate into the nucleus by 24 h. Over a more prolonged incubation period (48 h) DOX molecules were eventually located in the nuclear fraction and became more evident than 24 h of incubation. Almost only little DOX was observed in the cytoplasmic fraction, indicating that maximum DOX molecules from PEGylated PdNPs solely located in nuclear fraction at 48h incubation. Thus the nuclear drug concentration obtained with DOX conjugated PEGylated PdNPs clearly surpasses the concentration obtained with free DOX, especially after 48 h of incubation. The enhanced uptake of DOX conjugated PEGylated PdNPs can be attributed to their facilitated endocytotic transport, relative to passive diffusion of free DOX through the cell membrane.

4.6. *Fluorescence Microscopic studies*

4.6.1. AO/EtBr staining for detection of apoptotic cells.

The induction of apoptosis, after the treatment with IC_{50} concentrations of DOX conjugated PEGylated PdNPs for 24 and 48 h was assessed by fluorescence microscopy after staining with acridine orange/ ethidium bromide (AO/EtBr). The images of untreated and DOX

conjugated PEGylated PdNPs treated HeLa cells are presented in Fig.9a. The fluorescence microscopic analysis demonstrated that untreated HeLa cells were stained with a uniform green fluorescence. Because AO can penetrate the normal cell membrane, the cells without treatment were observed as green fluorescence. In contrast the apoptotic cells formed as a result of nuclear shrinkage, blebbing were observed as orange colored bodies due to their loss of membrane integrity when viewed under fluorescence microscope.[65]

4.6.2. DAPI staining for nuclear morphology study

This study dealt with the effect of DOX conjugated PEGylated PdNPs on HeLa cancer cells. DAPI staining of the nuclei for observation of nuclear morphology helps to distinguish the apoptotic nuclei from healthy ones. As seen from the images in Fig.9b normal HeLa cells had normal morphology with intact round nucleus emitting a weak florescence. However, on treatment with PdNPs, there was significant nuclei fragmentation with condensed and apoptotic nuclei (apoptotic nuclei shown by arrows). Fig. 9c shows that the total number of apoptotic cells increases when the incubation time increases .It has been reported that doxorubicin interacts with DNA topoisomerase II (topo II) causing the accumulation of enzyme-DNA adducts that ultimately lead to double-strand breaks and cell death via apoptosis.[66] Similar behavior of nuclei fragmentation was noticed by us when HeLa cells were treated with DOX-conjugated PEGylated PdNPs.

4.7. Effect of DOX-conjugated PEGylated PdNPs on intrinsic apoptosis

Cell death via apoptosis is an important event involved in a number of immunological processes. As most of the anticancer drugs are believed to trigger apoptosis *via* mitochondria-mediated pathway,[67,68] we here hypothesize that, as a new hybrid system, DOX-conjugated PEGylated PdNPs might also initiate the apoptosis *via* mitochondria- mediated pathway. Under this premise, we studied the changes of the levels of the mitochondrial-dependent apoptotic

proteins, including the caspase-3, the most important effector caspase, caspase-9, Bcl-2 and cytochrome *c*. Previous studies demonstrated that down regulation of anti-apoptotic protein Bcl-2 leads to release of cytochrome *c* from the mitochondria to cytosol, which is an essential step in the induction of apoptosis. Cytochrome *c* release from mitochondria to cytosol in turn leads to the activation of the caspase cascade such as caspase-3 and 9 which is critical in executing apoptosis, as it is either partially or totally responsible for the proteolytic cleavage of many key proteins.[69] Thus it is remarkable to speculate the analysis of Bcl-2, cytochrome C, and caspases-3 and 9 gene expressions. The results (Fig. 10) revealed a significant decrease in the expression of Bcl-2 and with an significant increase in the expression of cytosolic cytochrome C and caspase- 3 and 9 in cells treated with DOX conjugated PEGylated PdNPs compared to untreated control.

4.8. Hemolysis activity

Determination of hemolytic properties is one of the most common tests in studies of nanoparticle interactions with blood components.[70] Erythrocyte interaction with nanoparticles is particularly important in the application of nanoparticles for biological applications.[71] Two different methods were used to assess the hemolytic potential of PEGylated PdNP and DOX conjugated PEGylated PdNP; hemoglobin release analysis and cell morphology analysis. The RBCs were exposed to each NP sample for 3 h. Hemoglobin release analysis (Table. S2) shows the hemolytic activity of control, PEGylated PdNP and DOX conjugated PEGylated PdNP. When water is added to RBCs, hemolysis takes place and the released haemoglobin is measured. This serves as a positive control and represents absorbance to be 3.14 ± 0.062 (100% haemolysis). When, PEGylated PdNP and DOX conjugated PdNP was added, hemolysis was found to be less than 5% and are comparable to that suspended in PBS with absorbance of 0.02 ± 0.003 (0% hemolysis) which acts as a negative control. Fig. 11a shows photographs of the

hemolytic test on both the nanoparticle samples. The supernatant from PEGylated PdNP and DOX conjugated PdNP at different concentrations is achromatic, implying that no significant hemolysis occurred. It has been reported that up to 5% hemolysis is permissible for biomaterials.[72] Thus, both PEGylated PdNP and DOX conjugated PEGylated PdNP at the tested concentration exhibited no significant hemolysis. The largest percentage hemolysis obtained was 1.44±0.027% for 200µg/mL PEGylated PdNP and 1.57±0.054% for DOX conjugated PEGylated PdNP at 8µg/mL DOX concentration. Since this is much lower than 5%, it indicates that both PEGylated PdNP and DOX conjugated PEGylated PdNP are hemocompatible for drug delivery applications. The cell morphology analysis (Fig. 11b) corroborated the hemoglobin release analysis results. The cell morphology analysis indicated that incubation of RBCs with 200 μg/mL PEGylated PdNP and DOX conjugated PEGylated PdNP (8µg/mL DOX concentration) did not result in hemolysis or change in morphology of red blood cells when compared to control. Yu-Shen Lin *et al.*[73] showed the influence of PEG surface coating on hemolytic activity of mesoporous silica nanoparticle (MS NPs). The authors report that contrary to bare MS NPs, no apparent hemolysis was observed for PEG-coated MS NPs after 3 h blood incubation. In our study, the absence of hemolysis maybe due to biocompatible polymer PEG coating which prevented the adhesion of both the NPs to red blood cell membrane. Thus this simple surface modification stratagem is critical to ensure the safety of DOX conjugated PEGylated PdNP in biomedical applications.

4.9. *In Vivo* Anti-tumor Activity

In order to conform the feasibility of DOX-conjugated NPs for cancer therapy *in vivo*, the normal saline, DOX conjugated PEGylated PdNPs, PEGylated PdNPs and free DOX were injected at a dose of 5 mg DOX/kg body weight through the tail vein of the mice bearing cervical carcinoma HeLa cells and the anti-tumor activity of NPs was assessed. Here, the tumor volume

was recorded for a period of 18 days after the start of treatment, and mice injected with saline were treated as the control group. Fig. 12a shows the tumor growth curves after 18th day of treatment. The tumor volume of mice receiving normal saline, PEGylated PdNPs, rapidly increased at the end of 18th day and was observed to be 1102.27 ± 0.12 mm^3 and 1050.03 ± 1.67 mm^3, respectively. There were no significant differences of the tumor inhibition rate among the groups treated with normal saline solution and PEGylated PdNPs. It was clearly indicated that the growth of tumor was significantly (*$p < 0.05$) suppressed by the treatment of DOX conjugated PEGylated PdNPs and free DOX group when compared to the respective normal saline group. These results indicated that DOX conjugated PEGylated PdNPs could improve DOX delivery into the HeLa tumor by passive targetting. Moreover, the tumor growth suppression volume of the DOX conjugated PEGylated PdNPs group was 164.74 ± 0.17 mm^3 than that of the free DOX group 500.02 ± 1.34 mm^3, indicating the enhanced anti-tumor activity of DOX conjugated PEGylated PdNPs. The high antitumor activity of the DOX conjugated PEGylated PdNPs can be attributed to a higher accumulation in cancer cells, a controlled release feature and a decreased influence of MDR effect, as suggested earlier. Thus we inferred that DOX conjugated PEGylated PdNPs are uptaken by the tumor cells *via* an endocytic process. Once entering the cells, DOX is released from the DOX conjugated PEGylated PdNPs triggered by the acidic endocytic environment thereby greatly enhancing the anti-tumor activity. It is reported that the delivery of targeted NPs facilitates gradual accumulation of NPs in tumor tissue *via* endocytosis resulting in a potent anti-tumor activity. However, non-conjugated NPs remain in extracellular matrix of the tumor tissue and undergo degradation or phagocytosis, resulting in release of the drug. The results are nearly similar as those reported elsewhere.[74] As summarized in Fig.12a, although the tumor growth was inhibited after DOX conjugated PEGylated PdNPs

682 treatment, it is critical to evaluate the mice body weight loss. The fluctuation in animal body
683 weight is recognized as a useful indicator to assess in vivo toxicity of drug delivery systems.
684 Mice administrated with saline showed a steadily increasing body weight. Similar to the control
685 group, mice administered with blank PEGylated PdNPs and DOX conjugated PEGylated PdNPs
686 exhibited no decline in body weight, indicating the nontoxicity of the NPs. In contrast, the body
687 weight of DOX treated group of animals sharply decreased, compared to control and DOX
688 conjugated PEGylated PdNPs groups, (Fig. 12b), suggesting that toxic side effects were induced
689 by DOX at the given dose. Further, histological analysis of mice treated with normal saline,
690 PEGylated PdNPs and DOX conjugated PEGylated PdNPs revealed no significant signal of
691 damage from H&E stained organ slices including liver, heart, kidney, lung, and spinal cord (Fig.
692 12c). However, for group treated with DOX, acute inflammatory cell infiltration with obvious
693 organ damage of necrosis were apparent in heart and kidney tissues compared with the muscle
694 fibers and organ structure from control mice. These findings indicated that free DOX was
695 delivered not only in tumor cells but also to other normal cells and caused side effects; whereas
696 DOX conjugated PEGylated PdNPs can reduce assorted side effects. It is expected that most
697 DOX conjugated with PEGylated PdNPs will remain on the particle surface *via* a pH sensitive
698 hydrazone bond for a considerable length of time in the blood at normal physiological conditions
699 (pH 7.4), which greatly reduces the exposure of DOX to normal tissues and thus decreased the
700 toxicity and adverse side effect of DOX while effectively enhancing its anticancer activity.[75]
701
702 ## *5. Conclusion*
703 To our knowledge, this is the first report on using PEGylated PdNPs as drug delivery
704 system to deliver a chemotherapeutic agent into cancer cells. In conclusion, we have developed
705 as a proof of concept, a novel pH-responsive DOX conjugated PEGylated PdNPs as a new

delivery vehicle. For the first time, that the use of PEG as caps on the surface of palladium nanocarrier provides a suitable method for the design of delivery system able to selectively release conjugated cargos in responsive to cancer cells. The uniqueness of this drug delivery NP system is that the DOX was linked through pH-sensitive hydrazone bond to the hydrazide moity of PEGylated PdNPs. These NPs had well-controlled DOX loading yield, enhanced cellular uptake properties and showed excellent pH responsive drug release kinetics, leading to enhanced *in vitro* and *invivo* cytotoxicity against HeLa cells as compared to free DOX. As an environmentally sensitive drug delivery vehicle, these NPs can potentially minimize the drug loss during their circulation in the blood, where the pH value is neutral, and trigger rapid intracellular drug release when the NPs are endocytosed by the target cells. This characteristic drug release kinetics may suppress cancer cell chemoresistance and improve the therapeutic efficacy of the drug payload. In summary, the proposed new family of DOX conjugated PEGylated PdNP mediated drug delivery system has potential for tumor targeting and controlled release.

Conflict of interest

No conflict of interest was reported by the author of this article.

Acknowledgments

This research work was partially supported by UGC - Basic Science for Research (BSR) - RFSMS (Ref. G2/ 3142/ UGC – BSR – RFSMS / 2013) and DST-Nano-mission Project, Department of Science and Technology, Nano-mission division, New Delhi (Ref. SR/NM/NS-60/2010 dt. 08-07-2011).

References

1. S. Kayal, R.V. Ramanujan, *Mater. Sci. Eng., C.* 2010, 30, 484–490.
2. H.Yang, S.Y. Fung, M. Liu, *Angew. Chem. Int. Ed.* 2011, 50, 9643 –9646.
3. D.A. Gewirtz, M.L. Bristol J.C. Yalowich, *Curr. Opin. Invest. Drugs*. 2010, 11, 612−614.

4. M. Ferrari, *Nature Rev. Cancer.* 5, 2005, 161–171.
5. W. Von Rybinski, M.J. Schwuger, 1987. Adsorption and wetting, in: M. J. Schick (Ed.), Nonionic Surfactants: Physical Chemistry, Surfactant Sci. Ser., vol. 23, Marcel Dekker, New York.
6. K.E. Bremmell, S.R. Biggs, G.J. Jameson, *Colloids Surf. A.* 1999,146, 75-87.
7. K.Sathish kumar, J. Madhusudhanan, R.A. Thanigaivel, V.A. Veni, *Res. J. Biotech.* 2013, 8, 70-77.
8. J.Z. Du, X.J. Du, C.Q. Mao, J. Wang, *Am. Chem. Soc.* 2011.133, 17560−17563.
9. T. Zhou, C. Xiao, J. Fan, S. Chen, J. Shen, W. Wu, S. Zhou, *Acta Biomater.* 2013, 9, 4546−4557.
10. Y. Zhu, J. Shi, W. Shen, X. Dong, J. Feng, M. Ruan, Y. Li, *Angew. Chem., Int. Ed.* 2005, 117, 5213−5217.
11. W.H. Chiang , V.T. Ho, W.C. Huang, Y.F. Huang, C.S. Chern, Chiu HC. *Langmuir*. 2012, 42, 15056−15064.
12. D. Hua, J. Jiang, L. Kuang, J. Jiang, W.Zheng H. Liang, *Macromolecules*. 2011, 44, 1298-1302.
13. R. Liu, P. Liao, J. Liu, P. Feng, *Langmuir.* 2011,27, 3095-3099.
14. L.E. Gerweck, K. Seetharaman, *Cancer Res.* 1996, 56, 1194−1198.
15. H. Sun, B. Guo, X. Li, R. Cheng, F. Meng, H. Liu, Z. Zhong, *Biomacromolecules*. 2010, 4, 848−854.
16. W. Gao, J.M. Chan, O.C. Farokhzad, 2010, 6, 1913−1920.
17. D. Wang, X. Huan, L. Zhu, J. Liu, F. Qiu, D. Yan, X. Zhu, *RSC Adv.* 2012, 2, 11953−11962.
18. X. Hu, X. Hao, Y. Wu, J. Zhang, X. Zhang, P.C. Wang, G. Zou, X.J. Liang, *Mater. Chem. B.* 2013, 1, 1109−1118.
19. A. Popat, J. Liu, G.Q.M. Lu, S.Z.J. Qiao, *Mater.Chem*. 2012, 22, 11173−11178.
20. P. Tobiska, O. Hugon, A. Trouillet, H. Gagnaire, Sensors and Actuators B. 2001, 74, 168-172.
21. Z.H. Chen, J.S. Jie, L.B. Luo, H. Wang, C.S. Lee, S.T. Lee, *Nanotechnology*. 2007, 34, 345502.
22. P.R. West, S. Ishii, G.V. Naik, N.K. Emani, V.M. Shalaev, *Boltasseva A,* 2010, 6, 795-808.

763 23. J.L. Malleron, J.C. Fiaud, J.Y. Legros (2000) Handbook of palladium-catalyzed organic
764 reactions. London: Academic.
765 24. M.O.Nutt, J.B.Hughes, S.W.Michael, *Environ Sci Technol*, 2005, 39, 1346–53.
766 25. F. Favier, E.C. Walter, M.P. Zach, T. Benter, R.M. Penner, *Science*, 2001, 293, 2227–31.
767 26. S. Yu, U. Welp, L.Z. Hua, A. Rydh, W. K. Kwok, et al, *Chem Mater*, 2005, 17, 3445–50.
768 27. Z.Chang, H.Fan, K.Zhao, M.Chen, P.He, et al, *Electroanalysis* , 2008, 20: 131–136.
769 28. C.P.Adams, K.A.Walker, S.O.Obare, K. M. Docherty, *Plos one,* 2014, 9(1) e85981.
770 doi:10.1371/journal.pone.0085981
771 29. J.W.Xiao, S. X. Fan, F. Wang, L. D.Sun, X.Y.Zheng and C.H. Yan, Nanoscale, 2014, 6,
772 4345
773 30. I. Eryazici, C.N. Moorefield, G.R. Newkome, *Chem. Rev*. 2008, 108, 1834-1895.
774 31. S.D. Cummings, Coord. *Chem. Rev*. 2009, 253,1495-1516.
775 32. G. Tamasi, M. Casolaro, A. Magnani, A. Sega, L. Chiasserini, L. Messori, C. Gabbiani,
776 S.M. Valiahdi, M.A. Jakupec, B.K. Keppler, M.B. Hursthouse, *R. Cini, J. Inorg. Biochem.*
777 2010, 104, 799-814.
778 33. A. Divsalar, A.A. Saboury, H. Mansoori-Torshizi, F. Ahmad, *J. Phys. Chem. B*. 2010, 114,
779 3639-3647
780 34. E. Ulukaya, F. Ari, K. Dimas, E. I. Ikitimur, E. Guney, V. T. Yilmaz, *Eur. J. Med. Chem.*
781 2011,46, 4957-4963
782 35. A. Abuchowski, T. Van Es, N.C. Palczuk, F.F. Davis, *J. Biol. Chem.* 1977, 252, 3578-3581.
783 36. L.T.M. Hoa, T.T. Dung, T.M. Danh, N.H. Duc, D.M.J. Chien, *Phys.Conf. Ser.* 2009, 187,
784 012048.
785 37. Y. Zhang, N. Kohler, M. Zhang, *Biomaterials*. 2002, 7, 1553-1561.
786 38. A. Di Marco, M. Gaetani, B. Scarpinato, *Cancer Chemother. Rep.* 1969, 53, 33-37.
787 39. T. Teranishi, M. Miyake, *Chem. Mater.* 1998, 10, 594-600.
788 40. X. Yang, Q. Li, H. Wang, J. Huang, L. Lin, W. Wang, D. Sun, Y. Su, J.B. Opiyo, L.
789 Hong, Y. Wang, N. He, L. Jia, J. *Nanopart. Res*. 2010, 12, 1589–1598.
790 41. P. Mulvaney, *Langmuir*. 1996, 12, 788-800.
791 42. C.C. Luo, Y.H. Zhang, Y.G. Wang, *J. Mol. Catal. A: Chem.* 2005, 229, 7-12.
792 43. K. Okitsu, H. Bandow, Y. Maeda, Y. Nagata, *Chem. Mater* 1996, 8, 315-317.
793 44. T. Yonezawa, K. Imamura, N. Kimizuka, *Langmuir.* 2001, 17, 4701-4703.

45. P. F. Ho, K. M. Chi, *Nanotechnology.* 2004, 15, 1059-1064.
46. S. Sudeshna, S. Dipankar, D. Piyali, L. Rima, S. Amitabha, *Tetrahedron*. 2009, 65, 4367–4374.
47. H. Huang, Q. Yuan, J.S. Shah, R.D.K. Misra, *Adv. Drug Delivery Rev.* 2011, 63, 1332–1339.
48. C. Wang, L. Feng, H. Yang, G. Xin, W. Li, J. Zheng, W. Tian, X. Li, *Phys. Chem. Chem. Phys.* 2012, 38, 3233–13238.
49. D.C. Litzinger, A.M.J. Buiting, N. Rooijen, L. Huang, *Biochim. Biophys. Acta.* 1994, 1190, 99-107.
50. H. Maeda, Y. Matsumura, *Crit. ReV. Ther. Drug Carrier Syst.* 1989, 6, 193-210.
51. C.Li, *Adv. Drug Delivery Rev.* 2002, 54, 695-713.
52. A. Mandala, V. Medaa, ,W.J. Zhang, K.M. Farhan, A. Gnanamani, *Colloids Surf., B*. 2012, 90, 191– 196
53. E. Illés, E. Tombácz, M. Szekeres, I.Y.Tóth, Á. Szabó, B. Iván, *J.Magn.Magn.Mater,* 2015, 380, 132–139.
54. C.Barrera, A. Herrera, Y.Zayas, C.Rinaldi, *J.Magn.Magn.Mater*. 2009, 321, 1397–1399.
55. C. He, Y. Hu, L. Yin, C. Tang, C. Yin, *Biomaterials.* 2010, 31, 3657–66.
56. F. Alexis, E. Pridgen, L.K. Molnar, O.C. Farokhzad, *Mol Pharm.* 2008, 5, 505–15.
57. P. Aggarwal, J.B. Hall, C.B. McLeland, M.A. Dobrovolskaia, S.E. McNeil, *Adv Drug Deliv Rev.* 2009, 61, 428–37.
58. S. Kayal, R.V. Ramanujan, *J. Nanosci. Nanotechnol*. 2010, 10, 1–13.
59. L. Wong, M. Kavallaris, V. Bulmus, *Polym. Chem.* 2011, 2, 385–393.
60. J. Bénard, J. Da Silva, M.C. De Blois, P. Boyer, P. Duvillard, E. Chiric, G. Riou, *Cancer Res.* 1985, 45, 4970-4979.
61. N.V. Cuong, J.L. Jiang, Y.L. Li, J.R. Chen, S.C. Jwo, M.F. Hsieh, *Cancers.* 2011, 3, 61-78.
62. Y. Bae, S. Fukushima, A. Harada, K. Kataoka, *Angew Chem Int Ed.* 2003, 42, 4640-4643.
63. E.R. Gillies, J.M.J. Frchet, *Bioconjugate Chem.* 2005, 16, 361-368.
64. L.Jing, X. Liang, X. Li, Y. Yang, Z. Dai, Acta Biomaterialia, 2013, 9, 9434–9441.
65. R. Vivek, R. Thangam, K. Muthuchelian, P. Gunasekaran, K. Kaveri, S. Kannan. *Process Biochem.* 2012, 47, 2405–2410.

66. S. Banalata, K. Sanjana, P. Devi, B. Rakesh, K. M. Tapas, P. Panchanan, D Dibakar, *ACS Appl. Mater. Interfaces.* 2013, 5, 3884−3893.
67. A.S., Don, P.J., Hogg, *Trends Mol Med.* 2004, 10, 372–378.
68. J.M. Grad, E. Cepero, L.H. Boise, *Drug Resist Updat*. 2001, 4, 85–91.
69. R. Vivek, R. Thangam, V. NipunBabu, C. Rejeeth, S, Sivasubramanian, P. Gunasekaran, K. Muthuchelian, S. Kannan, *ACS Appl. Mater. Interfaces*. 2014, 6, 6469-6480.
70. F.Y. Cheng, C. H. Su, Y. S. Yang, C. S. Yeh, C. Y. Tsai, C. L. Wu, M.T. Wu, D.B. Shieh, *Biomaterials.* 2005, 26, 729-738.
71. R.K. Kainthan, M. Gnanamani, M. Ganguli, T. Ghosh, D.E. Brooks, S. Maiti, J.N. Kizhakkedathu, *Biomaterials*. 2006, 27, 5377.
72. J. P. Singhal, A. R. Ray, *Biomaterials*. 2002, 23, 1139–45.
73. Y.S. Lin, C.L. Haynes, *J. am. chem. soc.* 2010, 132, 4834–4842.
74. S. Aryal, J.J. Grailer, S. Pilla, D.A. Steeber, S. Gong, *J. Mater. Chem*. 2009, 19, 7879–7884.
75. K.T. Oh, H. Yin, E.S. Lee, Y.H. Bae,. *J. Mater. Chem*, 2007, 17, 3987–4001.

Figure Legends

Scheme 1. Schematic illustration of the synthesis of PEGylated PdNPs by reduction of H_2PdCl_4 with sodium borohydride ($NaBH_4$) in presence of PEG-hydrazide and subsequent formation of hydrazone bond between the hydrazide moity of PEGylated PdNPs and carbonyl group DOX.

Fig. 1. (a) UV–*vis* spectrum of H_2PdCl_4 and PEGylated PdNPs. The inset shows a digital image of the as-prepared PEGylated Pd colloidal solution (dark brown) and H_2PdCl_4 solution (transparent yellow) before reaction. (b) UV–*vis* spectrum of pure DOX and DOX conjugated PEGylated PdNPs.

Fig. 2. XRD patterns of (a) PEGylated PdNPs and (b) DOX conjugated PEGylated PdNPs.

Fig. 3. TEM micrographs of PEGylated PdNPs and DOX conjugated PEGylated PdNPs. The particles are almost spherical in shape. The size of PEGylated PdNP ranged approximately

between 10- 20 nm and DOX conjugated PEGylated PdNPs presented a slightly large size of approximately 35-45 nm.

Fig. 4. FTIR spectrum of (a) PEGylated PdNPs, (b) DOX and (c) DOX conjugated PEGylated PdNPs.

Fig. 5. NMR spectrum of (a) PEGylated PdNPs and (b) DOX conjugated PEGylated PdNPs.

Fig. 6. Cumulative DOX release (%) profile from DOX conjugated PEGylated PdNPs at 37 °C under pH conditions 7.4, 6.8 and 5.5. The data points are average of at least three experiments. Bars represent the range over which the values were observed.

Fig.7. The cytotoxicities of free DOX and DOX conjugated PEGylated PdNPs against HeLa cells as determined by MTT assay. Cells were treated with designated regimes for 24 h and 48 h. Data represent mean ± SD. $*p < 0.05$ was considered statistically significant.

Fig. 8. Confocal microscopy images of HeLa cells incubated with DOX conjugated PEGylated PdNPs for 24 h and 48 h. For each panel, the images from left to right show differential interference contrast (DIC) image, DOX fluorescence in cells (red), cell nuclei stained by DAPI (blue), and overlays of the three images. DOX dosage was 2 μg/mL.

Fig. 9. Fluorescent microscopic images of IC_{50} concentration of DOX conjugated PEGylated PdNPs treated on HeLa cells. (a) Cells were stained with AO/EtBr staining to differentiate necrotic and apoptotic cells from one another. Note that untreated HeLa cells were stained with a uniform green fluorescence. In contrast the apoptotic cells were observed as orange colored bodies whereas the necrotic cells were observed to be red in color. (b) Cells were stained with DAPI to visualize nuclear morphology. Note that untreated cells as control contained round nuclei with homogeneous chromatin and exhibited a less bright blue color. The cells treated with DOX conjugated PEGylated PdNPs showed chromatin condensation, reduction of nuclear size,

nuclear fragmentation and the blue emission light in the apoptotic cells was much brighter. (c) Percentage of apoptotic cells were measured after HeLa cells were incubated with DOX conjugated PEGylated PdNP with IC_{50} concentration. Data represent mean ± SD. *$p < 0.05$ was considered statistically significant.

Fig. 10. Apoptosis induced by DOX conjugated PEGylated PdNPs treated HeLa cells confirmed by semi-quantitative RT-PCR analysis of apoptotic related gene expressions. Expression of Bcl-2, cytochrome C, and caspases-3 and 9 after treatments with DOX conjugated PEGylated PdNPs. DOX dosage was 0.5 μg/mL, 1.0 μg/mL and 2.0 μg/mL.

Fig. 11. Hemolysis assay on PEGylated PdNPs and DOX conjugated PEGylated PdNPs (a) Photographs of hemolysis of RBCs incubated with different concentrations of PEGylated PdNPs and DOX conjugated PEGylated PdNPs with different DOX concentrations. The presence of red hemoglobin in the supernatant indicates damaged RBCs. D.I. water (+) and PBS (-) are used as positive and negative control, respectively.(b) Microscopic image (magnification of 40×) of human RBC treated with PEGylated PdNPs (200µg/mL) and DOX conjugated PEGylated PdNPs (DOX concentration 8μg/mL). RBC without any treatment is used as control. No noticeable changes were observed for both the nanoparticles.

Fig.12. In vivo combination cancer therapy. (a) Tumor growth curves of four different groups of mice after various treatments (4 mice/group) show varying degree of tumor suppression until the end of 18th day. The extent of tumor suppression is higher in DOX conjugated PEGylated PdNPs treated group than others. (b) Mice weight changes of HeLa tumor xenografted nude mice. Error bars are based on standard errors of the mean. *$p < 0.05$ was considered statistically significant. (c) Images show HE stained sections of liver, heart, kidney, lung, and spinal cord of the mice after different treatments.

898 **Graphical abstract.** Schematic illustration of the possible mechanism of pH based drug delivery
899 system of DOX conjugated PEGylated PdNPs induced apoptosis in HeLa cells.

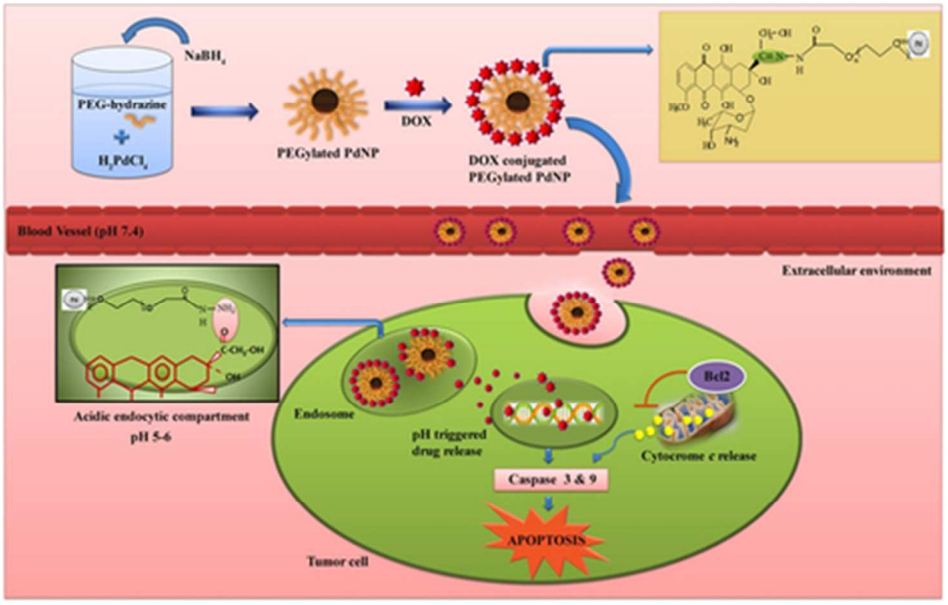

Schematic illustration of the possible mechanism of pH based drug delivery system of DOX conjugated PEGylated PdNPs induced apoptosis in HeLa cells.
39x25mm (300 x 300 DPI)

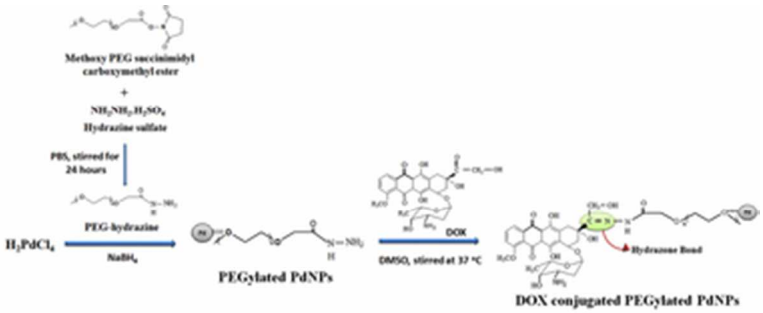

Scheme 1: Schematic illustration of the synthesis of PEGylated PdNPs by reduction of H2PdCl4 with sodium borohydride (NaBH4) in presence of PEG-hydrazide and subsequent formation of hydrazone bond between the hydrazide moity of PEGylated PdNPs and carbonyl group DOX.
32x12mm (300 x 300 DPI)

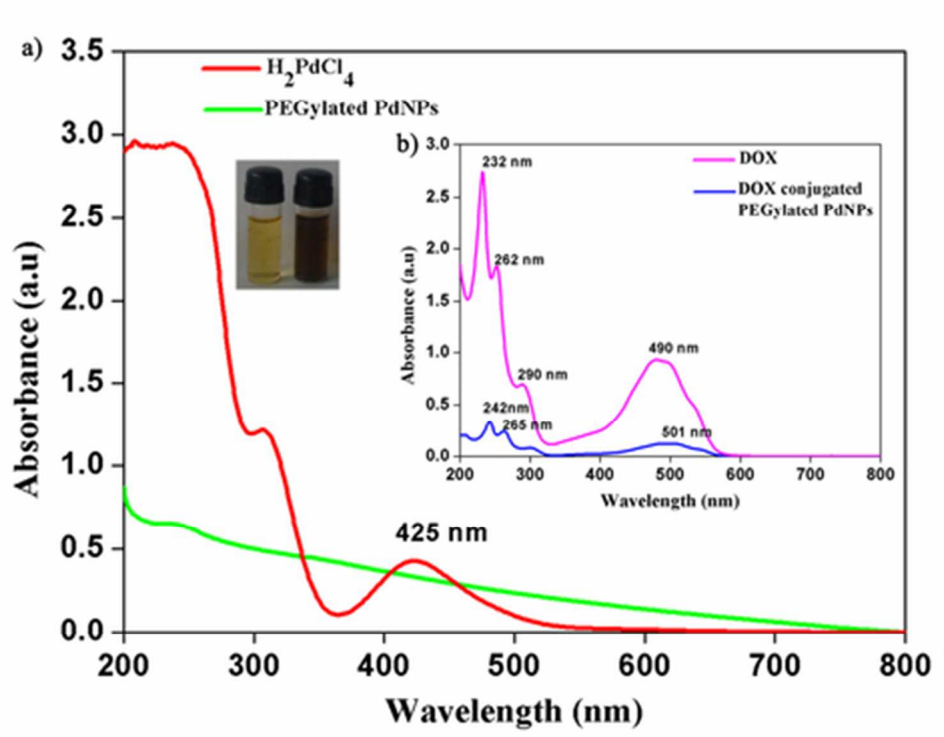

Figure 1: (a) UV–vis spectrum of H2PdCl4 and PEGylated PdNPs. The inset shows a digital image of the as-prepared PEGylated Pd colloidal solution (dark brown) and H2PdCl4 solution (transparent yellow) before reaction. (b) UV–vis spectrum of pure DOX and DOX conjugated PEGylated PdNPs.
39x31mm (300 x 300 DPI)

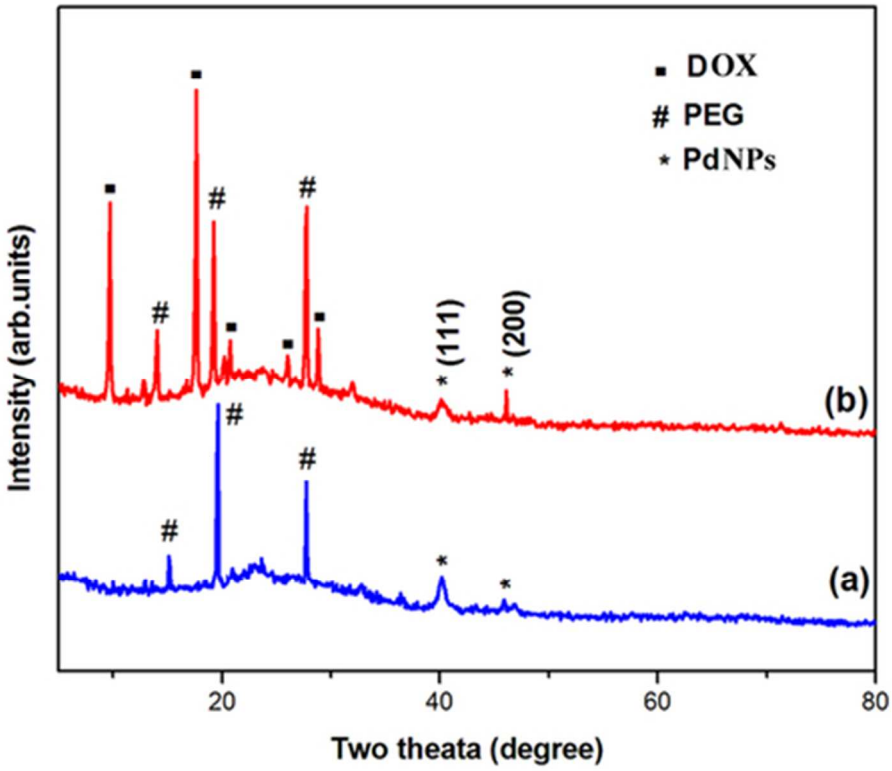

Figure 2: XRD patterns of (a) PEGylated PdNPs and (b) DOX conjugated PEGylated PdNPs.
39x33mm (300 x 300 DPI)

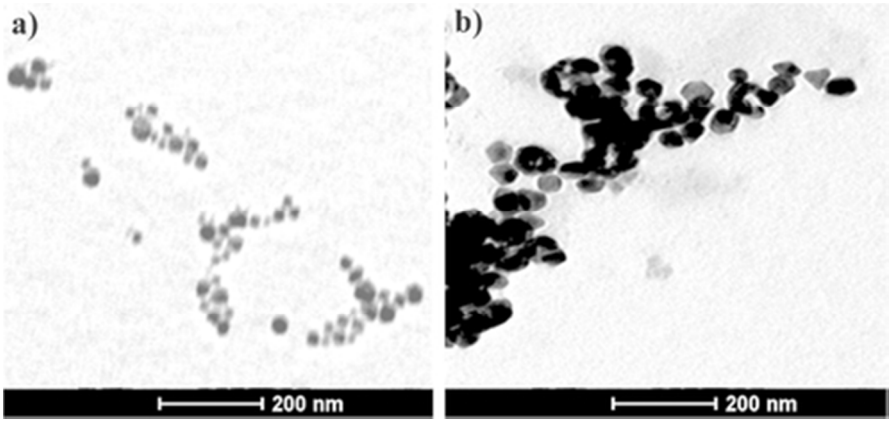

Figure 3: TEM micrographs of PEGylated PdNPs and DOX conjugated PEGylated PdNPs. The particles are almost spherical in shape. The size of PEGylated PdNP ranged approximately between 10- 20 nm and DOX conjugated PEGylated PdNPs presented a slightly large size of approximately 35-45 nm.
37x17mm (300 x 300 DPI)

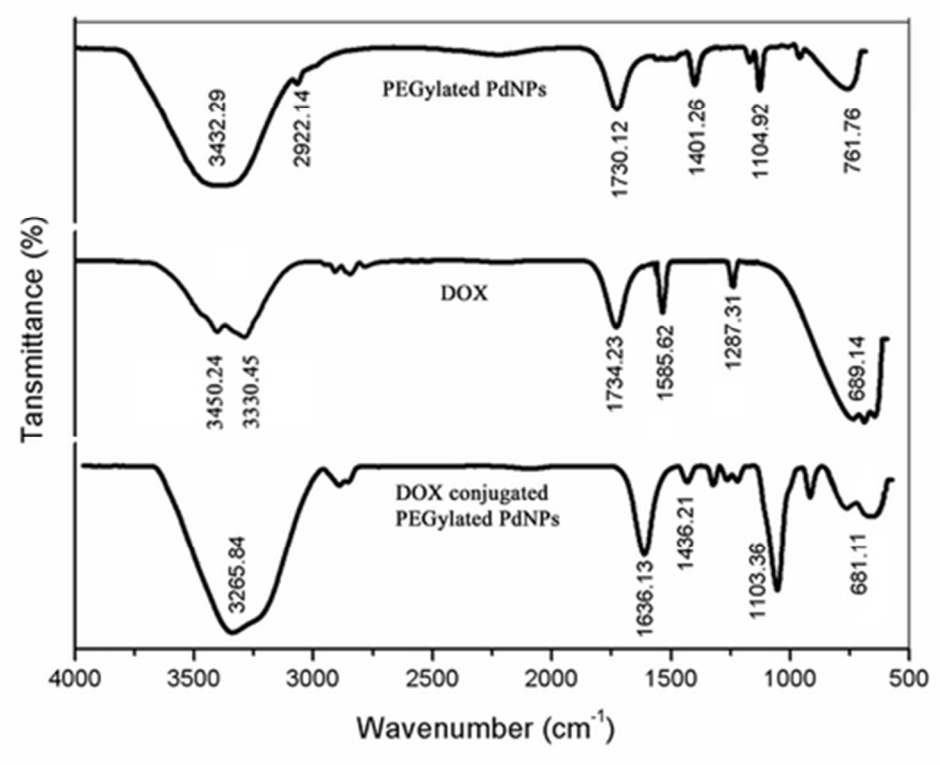

Figure 4: FTIR spectrum of (a) PEGylated PdNPs, (b) DOX and (c) DOX conjugated PEGylated PdNPs.
39x32mm (300 x 300 DPI)

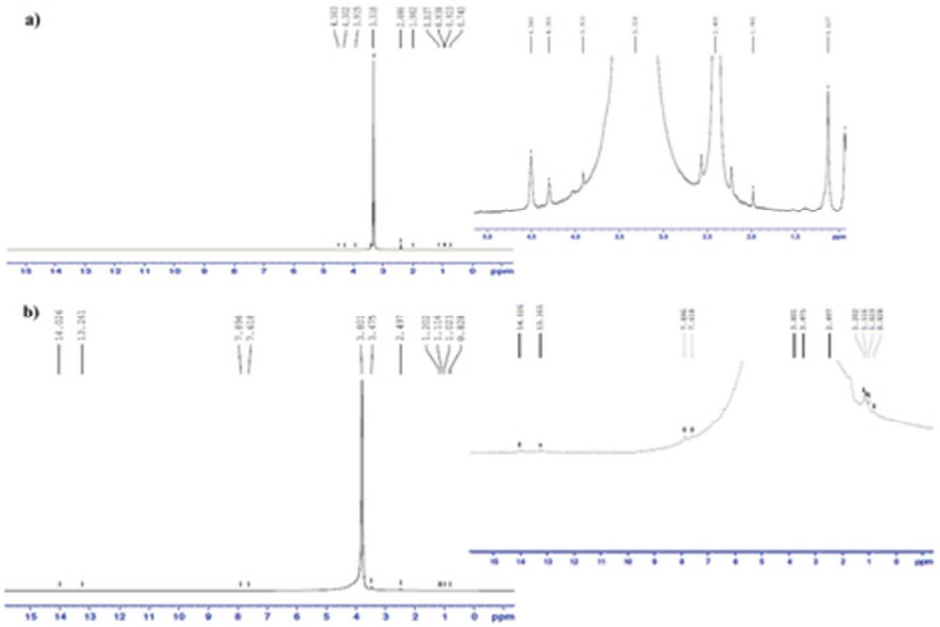

Figure 5: NMR spectrum of (a) PEGylated PdNPs and (b) DOX conjugated PEGylated PdNPs.
39x26mm (300 x 300 DPI)

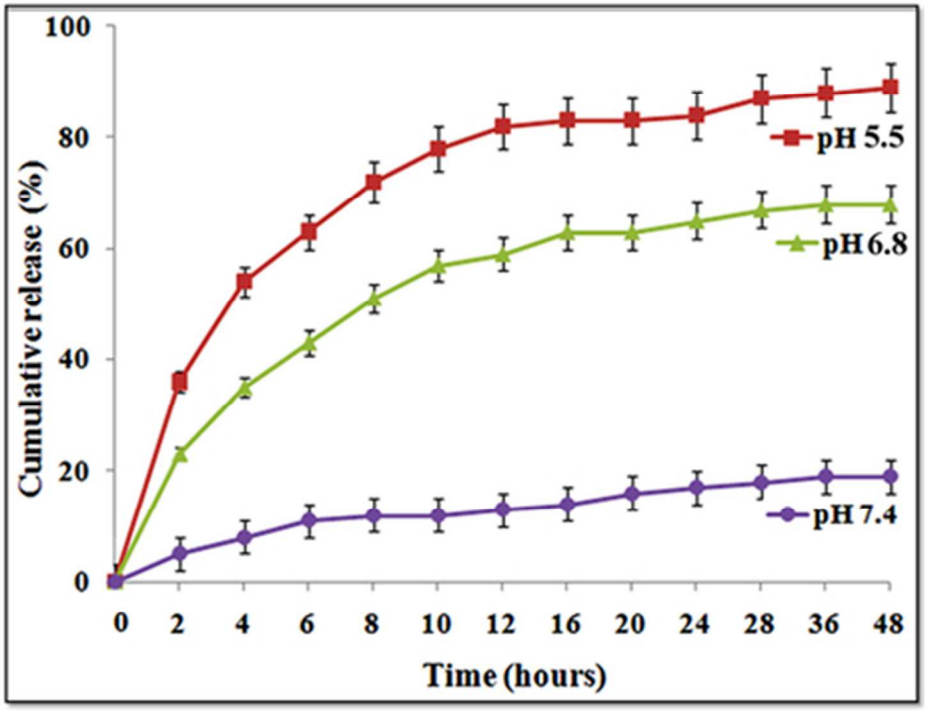

Figure 6: Cumulative DOX release (%) profile from DOX conjugated PEGylated PdNPs at 37 °C under pH conditions 7.4, 6.8 and 5.5. The data points are average of at least three experiments. Bars represent the range over which the values were observed.
39x30mm (300 x 300 DPI)

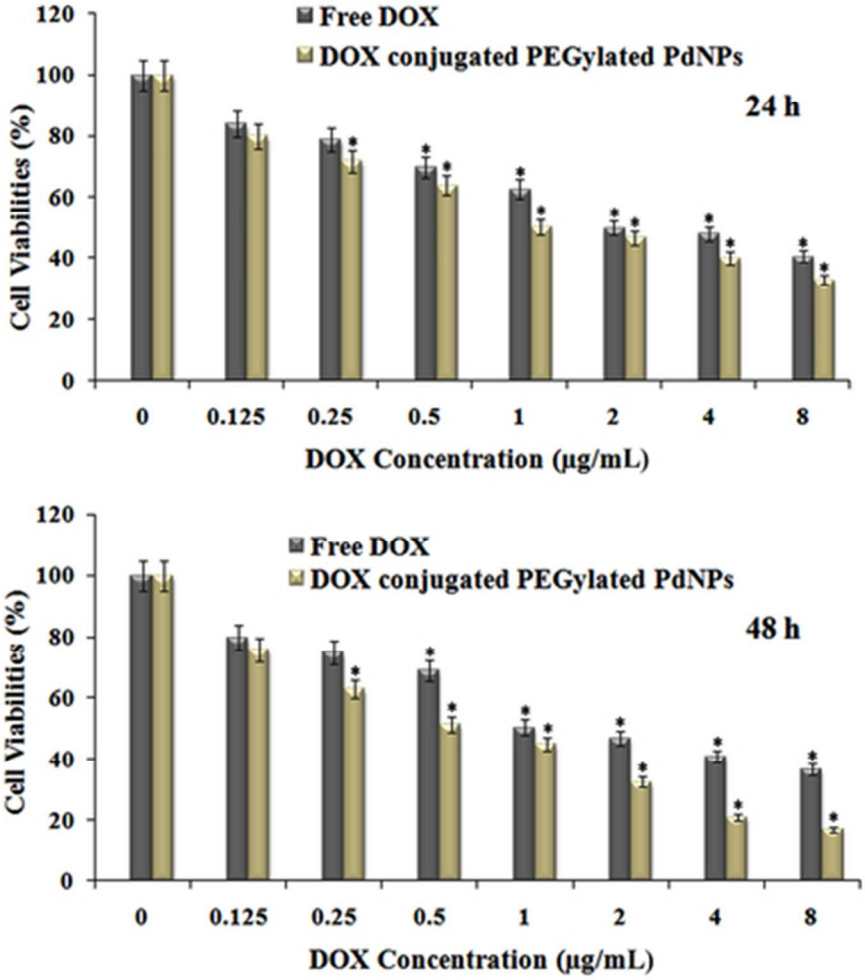

Figure 7: The cytotoxicities of free DOX and DOX conjugated PEGylated PdNPs against HeLa cells as determined by MTT assay. Cells were treated with designated regimes for 24 h and 48 h. Data represent mean ± SD. *p < 0.05 was considered statistically significant.
39x41mm (300 x 300 DPI)

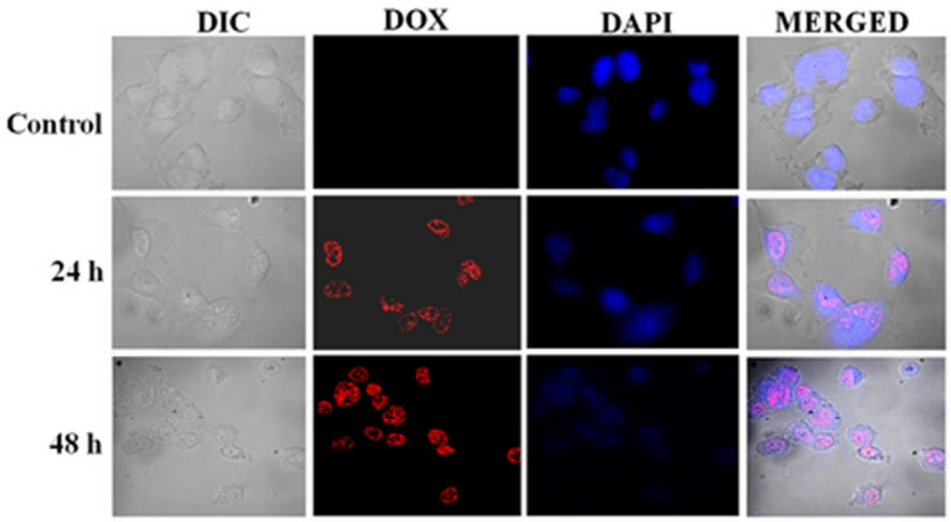

Figure 8: Confocal microscopy images of HeLa cells incubated with DOX conjugated PEGylated PdNPs for 24 h and 48 h. For each panel, the images from left to right show differential interference contrast (DIC) image, DOX fluorescence in cells (red), cell nuclei stained by DAPI (blue), and overlays of the three images. DOX dosage was 2 μg/mL.
39x21mm (300 x 300 DPI)

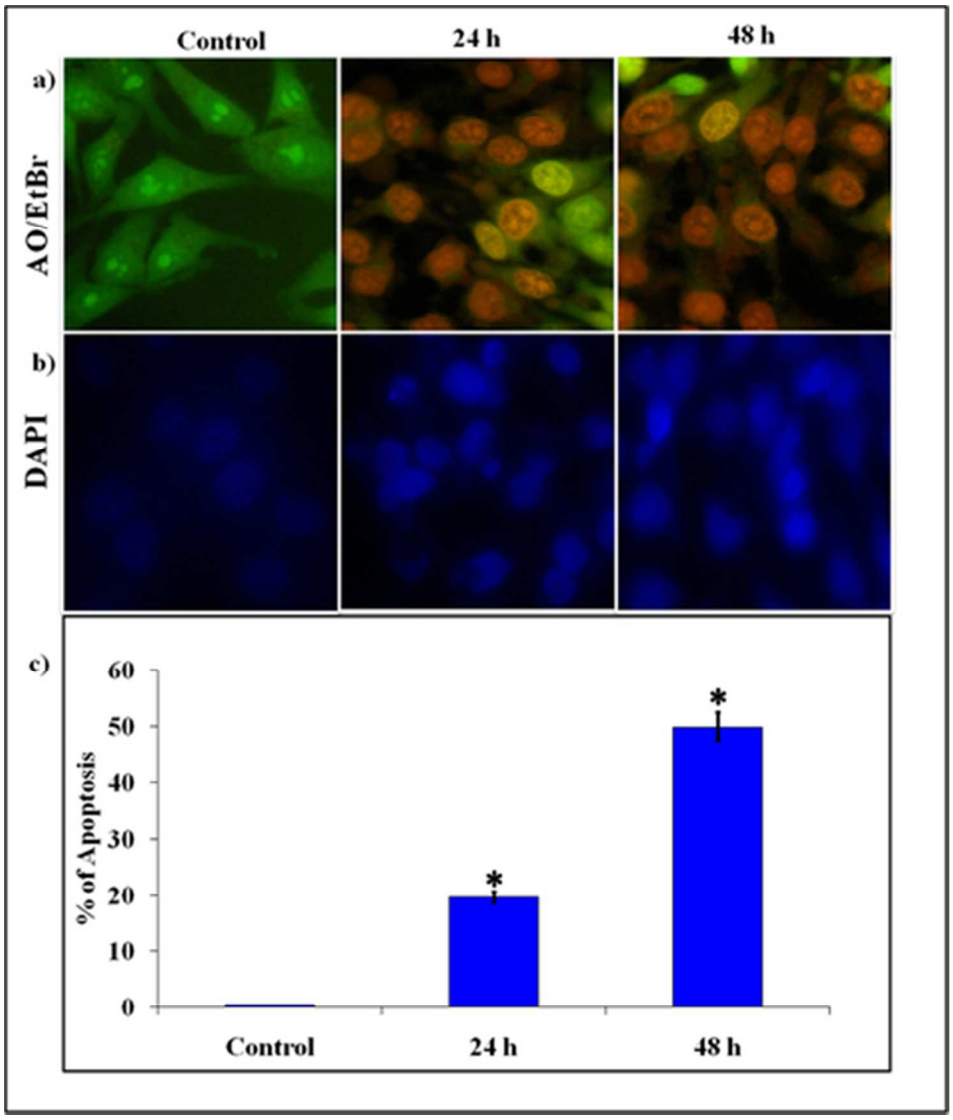

Figure 9: Fluorescent microscopic images of IC50 concentration of DOX conjugated PEGylated PdNPs treated on HeLa cells. (a) Cells were stained with AO/EtBr staining to differentiate necrotic and apoptotic cells from one another. Note that untreated HeLa cells were stained with a uniform green fluorescence. In contrast the apoptotic cells were observed as orange colored bodies whereas the necrotic cells were observed to be red in color. (b) Cells were stained with DAPI to visualize nuclear morphology. Note that untreated cells as control contained round nuclei with homogeneous chromatin and exhibited a less bright blue color. The cells treated with DOX conjugated PEGylated PdNPs showed chromatin condensation, reduction of nuclear size, nuclear fragmentation and the blue emission light in the apoptotic cells was much brighter. (c) Percentage of apoptotic cells were measured after HeLa cells were incubated with DOX conjugated PEGylated PdNP with IC50 concentration. Data represent mean ± SD. *$p < 0.05$ was considered statistically significant.
39x46mm (300 x 300 DPI)

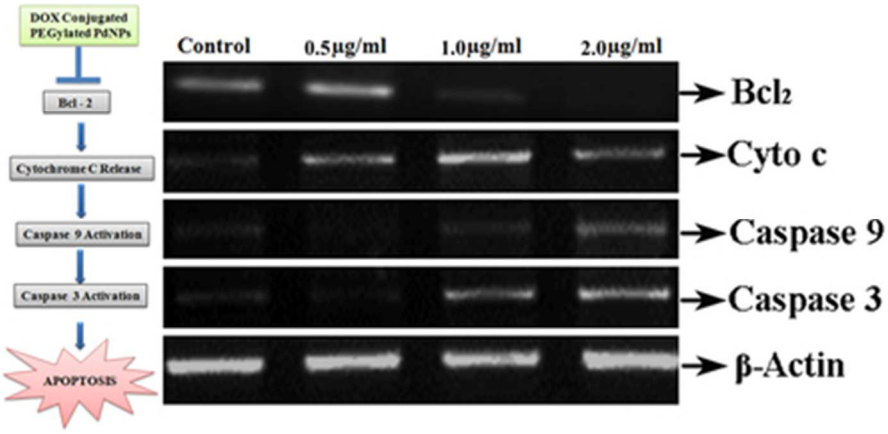

Figure 10: Apoptosis induced by DOX conjugated PEGylated PdNPs treated HeLa cells confirmed by semi-quantitative RT-PCR analysis of apoptotic related gene expressions. Expression of Bcl-2, cytochrome C, and caspases-3 and 9 after treatments with DOX conjugated PEGylated PdNPs.
DOX dosage was 0.5 µg/mL, 1.0 µg/mL and 2.0 µg/mL.

38x18mm (300 x 300 DPI)

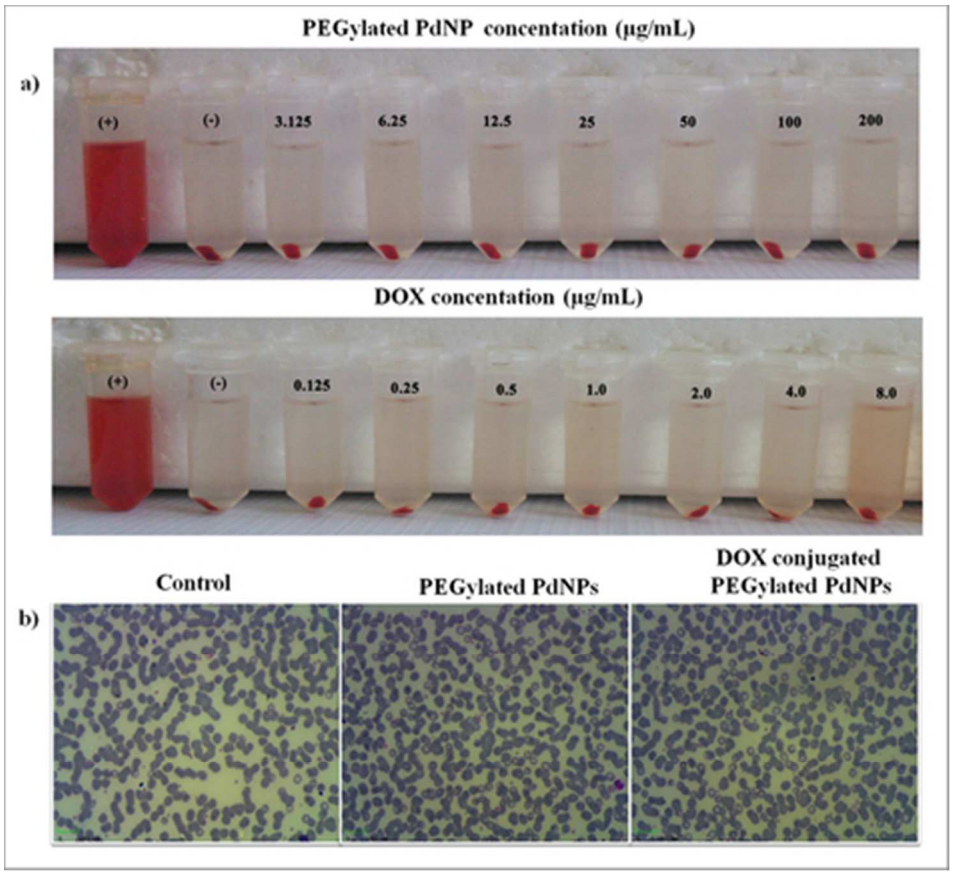

Figure 11: Hemolysis assay on PEGylated PdNPs and DOX conjugated PEGylated PdNPs (a) Photographs of hemolysis of RBCs incubated with different concentrations of PEGylated PdNPs and DOX conjugated PEGylated PdNPs with different DOX concentrations. The presence of red hemoglobin in the supernatant indicates damaged RBCs. D.I. water (+) and PBS (-) are used as positive and negative control, respectively.(b) Microscopic image (magnification of 40×) of human RBC treated with PEGylated PdNPs (200µg/mL) and DOX conjugated PEGylated PdNPs (DOX concentration 8µg/mL). RBC without any treatment is used as control. No noticeable changes were observed for both the nanoparticles.
39x36mm (300 x 300 DPI)

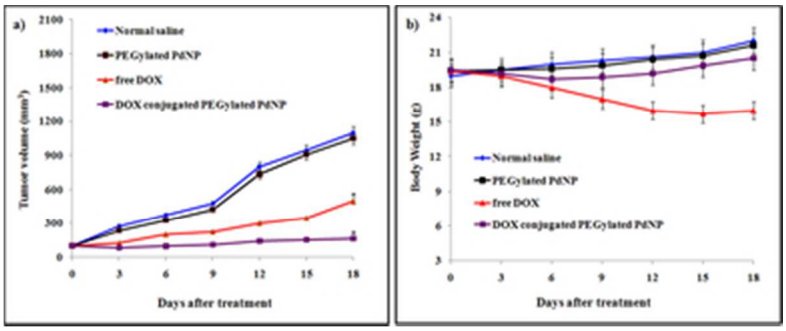

Figure 12a,b: In vivo combination cancer therapy. (a) Tumor growth curves of four different groups of mice after various treatments (4 mice/group) show varying degree of tumor suppression until the end of 18th day. The extent of tumor suppression is higher in DOX conjugated PEGylated PdNPs treated group than others. (b) Mice weight changes of HeLa tumor xenografted nude mice. Error bars are based on standard errors of the mean. *p < 0.05 was considered statistically significant.
32x13mm (300 x 300 DPI)